Journal of Asian Earth Sciences 219 (2021) 104890

Contents lists available at ScienceDirect

Journal of Asian Earth Sciences

journal homepage: www.elsevier.com/locate/jseaes

Early Paleozoic and Late Mesozoic crustal reworking of the South China Block: Insights from Early Silurian biotite granodiorites and Late Jurassic biotite granites in the Guangzhou area of the south-east Wuyi-Yunkai orogeny

Xiao Liu [a,c], Qiang Wang [a,b,c,*], Lin Ma [a,b,c,*], Jin-Hui Yang [d], Yi-Ming Ma [a,e], Tong-Yu Huang [a,c]

[a] State Key Laboratory of Isotope Geochemistry, Guangzhou Institute of Geochemistry, Chinese Academy of Sciences, Guangzhou 510640, China
[b] CAS Center for Excellence in Deep Earth Science, Guangzhou 510640, China
[c] College of Earth and Planetary Sciences, University of Chinese Academy of Sciences, Beijing 100049, China
[d] Institute of Geology and Geophysics, Chinese Academy of Sciences, Beijing 100029, China
[e] School of Earth Sciences, China University of Geosciences, Wuhan 430074, China

ARTICLE INFO

Keywords:
Granitoids
Continental crust reworking
Crust–mantle interaction
SE Wuyi-Yunkai orogen
South China

ABSTRACT

The South China Block (SCB) is considered to have undergone extensive reworking of continental crust. However, the processes and mechanisms of this reworking remain uncertain. Here, we investigated Early Silurian (442 Ma) biotite granodiorites and Late Jurassic (164–159 Ma) biotite granites in the Guangzhou area of SE Wuyi-Yunkai orogen (WYO), South China. The biotite granodiorites and biotite granites show major and trace element characteristics similar with crustal-derived melts. They have enriched whole-rock Sr–Nd (($^{87}Sr/^{86}Sr)_i$ = 0.7108–0.7210; $\varepsilon_{Nd}(t) = -11.7$ to -7.6) and zircon Hf ($\varepsilon_{Hf}(t) = -17.2$ to -1.7) isotopic compositions. Early Silurian biotite granodiorites have relatively homogeneous zircon $\delta^{18}O$ values (8.6‰–9.3‰) while Late Jurassic biotite granites show a wide range of zircon $\delta^{18}O$ values (7.4‰–10.6‰). We suggest that the Early Silurian biotite granodiorites were formed by partial melting of amphibolites and that the Late Jurassic biotite granites were formed by partial melting of a hybridized crustal source containing metasedimentary rocks with subordinate juvenile crustal rocks. Combining our results with those of previous studies in the SCB, we suggest that Early Paleozoic intracontinental reworking of the SCB can be divided into three stages: crust double-thickening, orogenic collapse, and post-orogenic lithospheric extension. During the Late Ordovician to Early Silurian, Guangzhou area of the SE WYO underwent reworking mainly of middle–lower-crustal rocks in response to crust double-thickening. In addition, during the Late Jurassic, the area underwent reworking mainly of middle–lower-crustal metasedimentary rocks, which was induced by heating from mantle-derived mafic magmas.

1. Introduction

Reworking of continental crust involves repeated metamorphism, deformation, and remelting of crustal rocks without a change in lithospheric-scale volume (Holdsworth et al., 2001). Such reworking may promote metal mineralization (Liu et al., 2020c) and remobilization of crustal carbon (Cheng, 2020; Mason et al., 2017), and is evidenced by the occurrence of folds, metamorphic rocks, and granitoids at Earth's surface. In addition, magmatic zircons in granitoids with elevated $\delta^{18}O$ (>8.0‰) or mantle $\delta^{18}O$ (5.3‰ ± 0.3‰) values are closely related to the reworking of supracrustal metasedimentary rocks or infracrustal juvenile crustal rocks, respectively (Zheng et al., 2007). Investigation of the reworking of continental crust is important in understanding the chemical composition and differentiation of crustal rocks (Hawkesworth and Kemp, 2006). Furthermore, reworking of continental crust is known to be associated with W–Sn–Nb–Ta mineralization (Shu et al., 2011; Mao et al., 2013a,b, 2021). The SCB is an natural laboratory to study continental crust reworking (Wang et al., 2013b; Shu et al., 2021). After the Neoproterozoic amalgamation of the Yangtze and Cathaysia blocks, the SCB underwent four major periods of reworking of continental crust,

* Corresponding authors at: State Key Laboratory of Isotope Geochemistry, Guangzhou Institute of Geochemistry, Chinese Academy of Sciences, Guangzhou 510640, China.
E-mail addresses: wqiang@gig.ac.cn (Q. Wang), malin@gig.ac.cn (L. Ma).

https://doi.org/10.1016/j.jseaes.2021.104890
Received 26 March 2021; Received in revised form 9 June 2021; Accepted 6 July 2021
Available online 9 July 2021

during the Neoproterozoic (Li et al., 2005), Early Paleozoic (Wang et al., 2013b; Shu et al., 2015), Early Mesozoic (Wang et al., 2007a), and Late Mesozoic (Zhou and Li, 2000; Li and Li, 2007). However, the mechanisms and processes of crustal reworking in the SCB are debated, especially with respect to the reworking during the Early Paleozoic and Late Mesozoic.

Three major mechanisms have been proposed to explain the reworking of continental crust of the SCB during the Early Paleozoic. (1) Crustal double-thickening was linked to intraplate subduction or overthrusting between the Cathaysia and Yangtze Blocks (Faure et al., 2009; Shu et al., 2015; Li et al., 2010). (2) Orogenic collapse followed by crust double-thickening (Yao et al., 2012; Wang et al., 2013c; Zhong et al., 2014, 2016); (3) The Early Paleozoic orogeny was formed by oceanic subduction and the subsequent collision between the west Cathaysia Terrane and a yet-unidentified terrane (Lin et al., 2018; Tong et al., 2021).

The SCB continental crust underwent its most intense episode of reworking during the Late Mesozoic, as evidenced by extensive Late Mesozoic granitic magmatism and mineralization (Zhou and Li, 2000; Zhou et al., 2006; Mao et al., 2013a,b). Late Mesozoic continental reworking mechanisms can be summarized into three types: (1) NW–WNW-directed oblique subduction and subsequent roll-back of Paleo-Pacific oceanic lithosphere (Zhou and Li, 2000; Jiang et al., 2009, 2015); (2) flat slab subduction and subsequent slab foundering (Li et al., 2007; Li and Li, 2007); (3) post-orogenic (Triassic: 252–201 Ma) lithospheric extension after collision of the SCB and Indochina and North China Blocks (Wang et al., 2003). Intensive large-scale reworking of the SCB continental crust required a heat supply from mantle-derived mafic magmas (Zhou and Li, 2000). However, whether reworking of metasedimentary rocks could be induced by such a heating mechanism in addition to *in situ* radiogenic heating related to over-thickened crust (Wang et al., 2007a; Shu et al., 2015) remains uncertain.

In this study, we present detailed petrographic, geochronological, whole-rock major- and trace-elemental, and whole-rock Sr–Nd and zircon Hf–O isotopic data for Early Paleozoic biotite granodiorites and Late Mesozoic biotite granites from the Guangzhou area of SE WYO, southeastern China. These data, together with results of previous studies, are used to provide insights into processes involved in the reworking of continental crust in the SCB during the Early Paleozoic and Late Mesozoic.

2. Geological background and sample descriptions

The SCB is bounded by the Pacific Ocean to the east, the

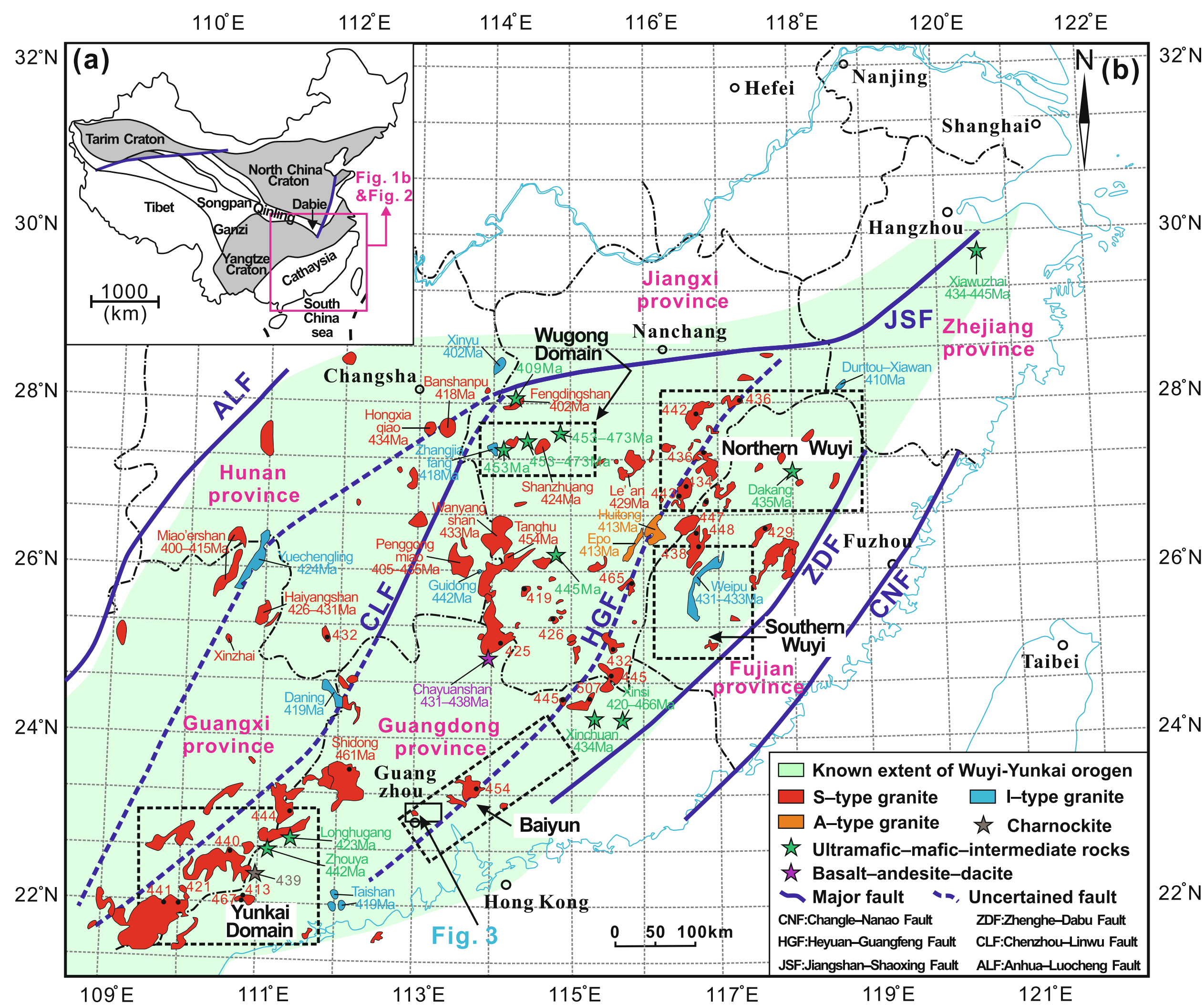

Fig. 1. (a) Simplified regional map showing the tectonic framework of China (revised from Liu et al., 2020a, and references therein). (b) Sketch map showing the distribution of Early Paleozoic WYO magmatic rocks in the South China Block (SCB) (modified after Liu et al., 2020a, and references therein). The solid blue line represents the Yangtze River or coastline. The dotted black lines are provincial borders. Ages and geochemical characteristics of representative Early Paleozoic magmatic rocks in the Guangdong province of southern Nanling Range are compiled in Supplementary Tables 5 and 6. (For interpretation of the references to colour in this figure legend, the reader is referred to the web version of this article.)

Longmenshan Fault Zone and Ailaoshan–Honghe Fault to the west, the Qinling–Dabie–Sulu ultrahigh-pressure tectonic belt to the north, and the South China Sea to the south (Fig. 1a). The SCB is composed of the Yangtze Block to the northwest and the Cathaysia Block to the southeast, which were amalgamated along a continent–continent collisional belt (the Jiangnan orogen) during the Neoproterozoic (980–820 Ma; Fig. 1a; Li et al., 2009a; Zhao, 2015; Shu et al., 2019, 2021). After the amalgamation of the Yangtze and Cathaysia Blocks, a Late Neoproterozoic failed rift with a > 13 km thick abyssal marine deposition was developed (Wang and Li, 2003). The rift successions in the Cathaysia Block mainly occur at the Wuyi-Baiyun-Yunkai Domains, geographically extending from Hunan, through Jiangxi and western Guangdong, to eastern Guangxi provinces (Wang et al., 2011, and references therein; Fig. 1b).

The Lower Paleozoic sedimentary rocks in the SCB are characterized by a siliciclastic succession in the Cathaysia Block and an interstratified carbonate-siliciclastic succession in the eastern Yangtze Block (Wang et al., 2011). A regionally extensive angular unconformity between the Upper Paleozoic terrestrial deposits and the underlying Lower Paleozoic metasedimentary rocks were identified in the southeastern part of the SCB (Wang et al., 2011). This angular unconformity, together with widespread Silurian granitic magmatism define the Early Paleozoic orogeny in the SCB (Huang et al., 2013b, and references therein). The Upper Paleozoic and Early Triassic sedimentary rocks in the SCB are limestone, dolomite, black chert, sandstone, and mudstone (Shu et al., 2015, and references therein). The end of Early Triassic sedimentation indicates the Middle-Late Triassic (240–200 Ma) orogeny in the SCB

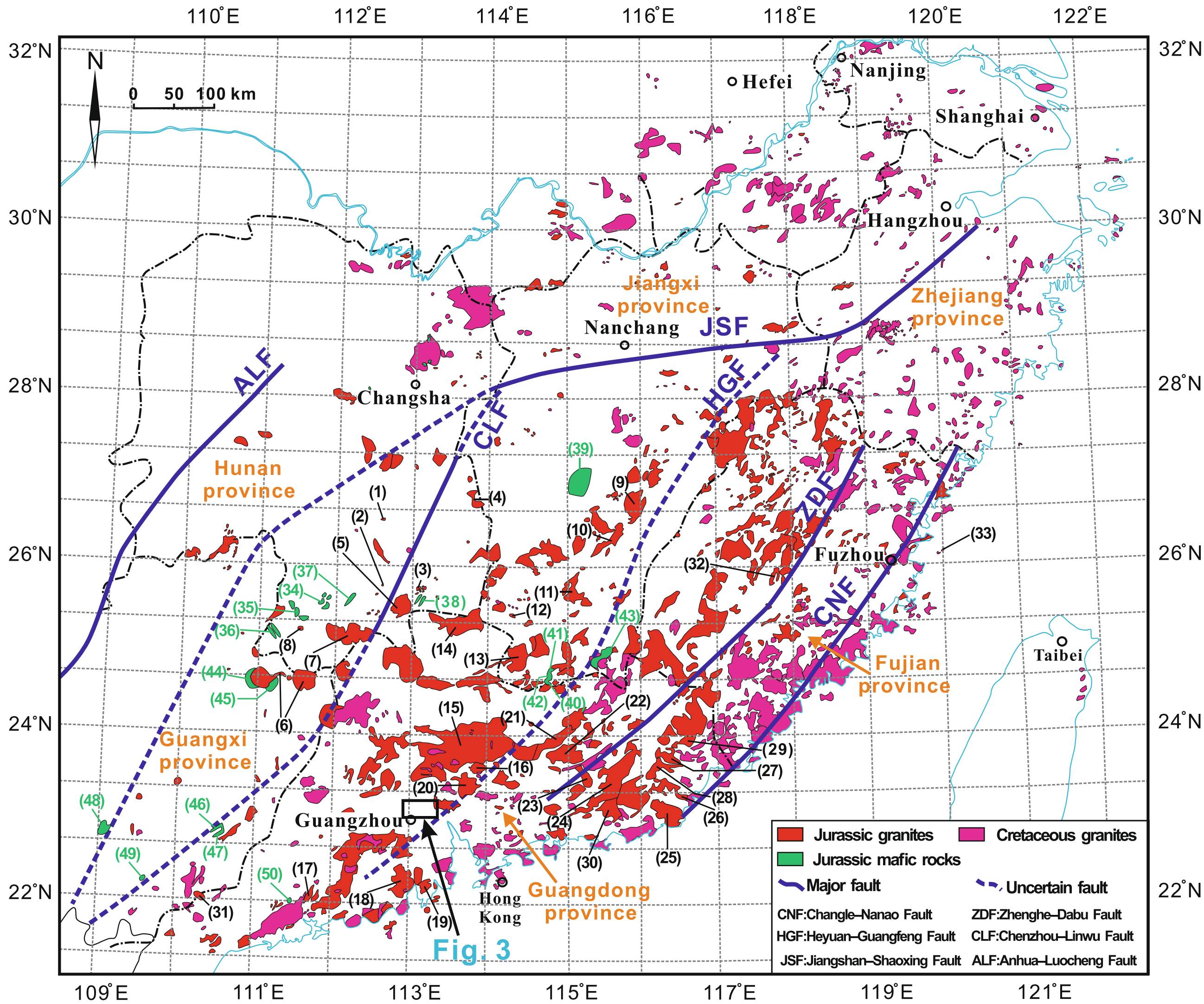

Fig. 2. Sketch map showing the location of Jurassic and Cretaceous granitic and Jurassic mafic rocks in the SCB (modified after Liu et al., 2020b, and references therein). Black and green numbers are representative Late Jurassic (ca. 160 Ma) granites and Middle to Late Jurassic mafic rocks, respectively (modified after Liu et al., 2020b, and references therein). (1) Shuikoushan (158 Ma); (2) Baoshan (158 Ma); (3) Qianlishan (163–153 Ma); (4) Xitian (154 Ma); (5) Qitianling (163–153 Ma); (6) Huashan–Guposhan (162 Ma); (7) Jiuyishan (or Jinjiling–Xishan, 154 Ma); (8) Tongshanling (164 Ma); (9) Taoshan (154 Ma); (10) Jiangbei (159–157 Ma); (11) Dabu (157 Ma); (12) Xihuashan (160–158 Ma); (13) Longyuanba (157 Ma); (14) Jiufeng (160–157 Ma); (15) Fogang (165–159 Ma); (16) Nankunshan (158 Ma); (17) Gangwei (166 Ma); (18) Gudoushan (161 Ma); (19) Wuguishan (160 Ma); (20) Lapu (163 Ma); (21) Xinfengjiang (161 Ma); (22) Baishigang (159 Ma); (23) Longwo (165 Ma); (24) Lianhuashan (165 Ma); (25) Wushikeng (160 Ma); (26) Chiliao (157 Ma); (27) Hulutian (159 Ma); (28) Mantoushan (164 Ma); (29) Fenghuang (161 Ma); (30) Shigushan (159 Ma); (31) Qinghu (160 Ma); (32) Tangquan (160 Ma); (33) Nankan Island (160 Ma); (34) Daoxian (176–174 Ma); (35) Ningyuan (154–150 Ma); (36) Huilongxu (172 Ma); (37) Zhicun (146 Ma); (38) Changchengling (178 Ma); (39) Antang (168 Ma); (40) Dongkeng (178 Ma); (41) Chebu (176–173 Ma); (42) Chenglong (182 Ma); (43) Baimianshan (173 Ma); (44) Tong'an (163 Ma); (45) Niumiao (161 Ma); (46) Yangmei (162 Ma); (47) Nandu (160 Ma); (48) Mashan (160 Ma); (49) Maqigang (160 Ma); (50) Ma–Shan (164 Ma). The solid blue line is the Yangtze River or coastline. The dotted black lines are provincial borders. Ages and geochemical characteristics of representative Mesozoic magmatic rocks in the Guangdong province of southern Nanling Range are compiled in Supplementary Tables 5–6. (For interpretation of the references to colour in this figure legend, the reader is referred to the web version of this article.)

(Wang et al., 2007a). Middle-Late Triassic orogeny caused large-scale folding and thrusting of pre-Triassic strata and formation of peraluminous granites (Wang et al., 2007a). The tectonic setting of the SCB gradually changed from compression to extensional during Late Mesozoic (Zhou et al., 2006). In the Jurassic and Cretaceous, the SCB was characterized by magma flare-ups, and 80% of the SCB igneous rocks (which have a total exposed area of > 200,000 km^2) were formed during this period (Li et al., 2007; Zhou et al., 2006).

Guangdong province is located in the southern Nanling Range in the Cathaysia Block (Fig. 1b and 2). Early Paleozoic granites are distributed chiefly in western Guangdong province (Yunkai domain) (Huang et al., 2013b; Wang et al., 2007b, 2011). In addition, minor Early Paleozoic granites are distributed in eastern (Ding et al., 2005), northern (Xu et al., 2005; Xie et al., 2020), and central (Yang et al., 2010; Liu et al., 2020a) Guangdong province. These granites are dominated by S-type granites with gneissic or massive texture that contain muscovite, garnet, or tourmaline (Wang et al., 2011; Liu et al., 2020a). Several granites are amphibole-bearing I-type granites that contain mafic microgranular enclaves (Huang et al., 2013b; Xie et al., 2020). Early Paleozoic granites in Guangdong province were emplaced mainly between 467 and 413

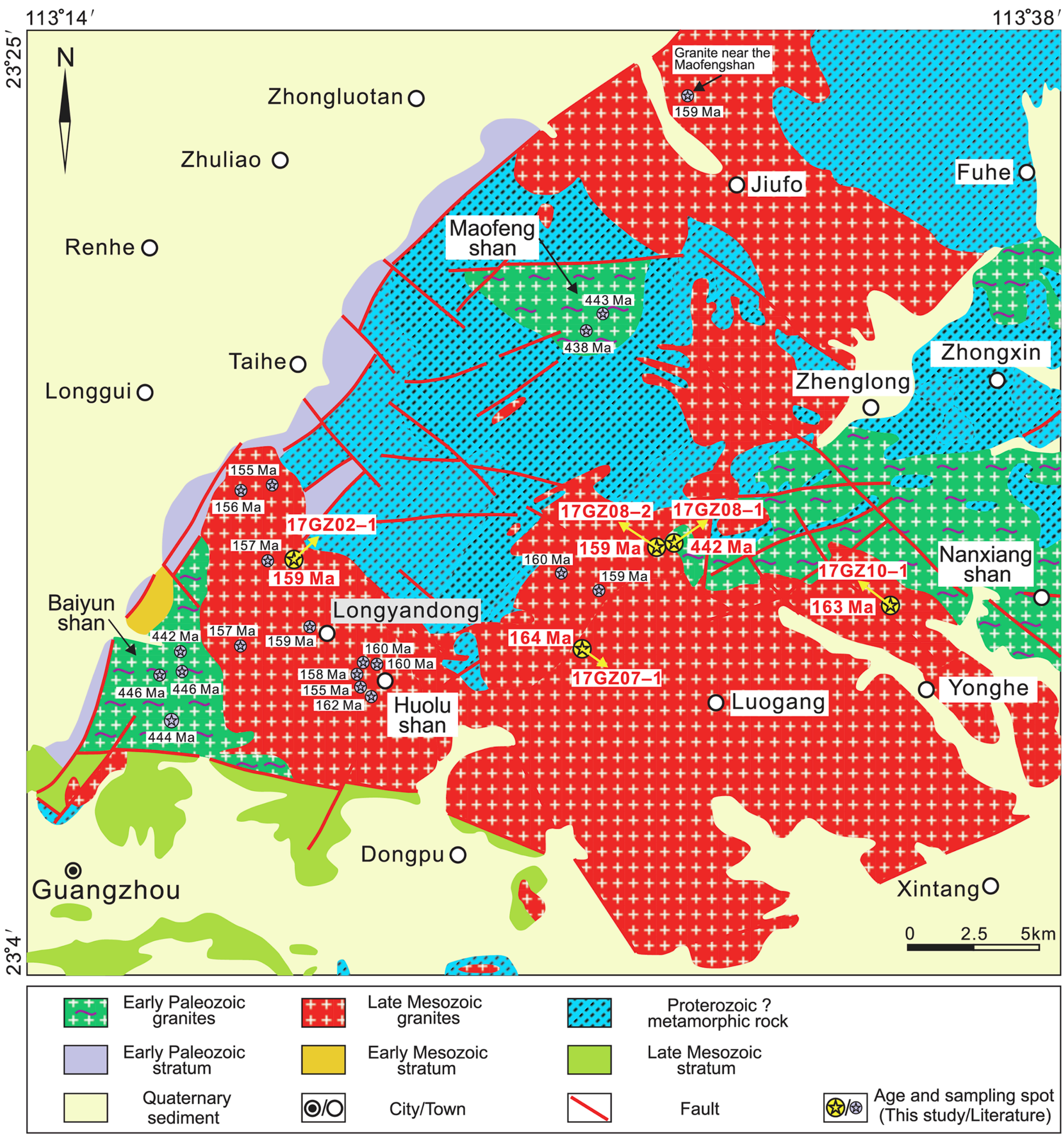

Fig. 3. Simplified geological map of the Guangzhou area, SE WYO (modified after Guangzhou Geological Maps at a scale of 1:250,000 (GDGBMR, 1988)), showing rock types and sample locations. Age data are from this study, Liu et al. (2020a, b, 2021), and Guo et al. (2019).

Ma, with an age peak of ca. 440 Ma (Supplementary Fig. 1). In addition to granites, Early Paleozoic gabbros (Wang et al., 2013c), volcanic rocks (basalts, andesites, and dacites; Yao et al., 2012), and charnockites (Wang et al., 2013a) crop out in northern and western Guangdong province (Liu et al., 2020a; Fig. 1b).

Early Mesozoic granites are distributed predominantly in western Guangdong province (Yunkai domain) (Peng et al., 2006; Zhou et al., 2006; Wang et al., 2013b; Qing et al., 2020) with a few in the northern part of the province (Chen et al., 2012; Gao et al., 2014). These granites are dominated by peraluminous granites that are composed of muscovite, garnet, and tourmaline (Chen et al., 2012; Wang et al., 2013b; Gao et al., 2017), along with minor A-type granites (Qing et al., 2020), and were formed between 245 and 204 Ma (Peng et al., 2006; Chen et al., 2012; Wang et al., 2013b; Qing et al., 2020). Late Mesozoic granites are distributed widely in Guangdong province (Fig. 2). Most of the granites are I-type or highly fractionated I- and A-type and associated with tungsten–tin polymetallic deposits in eastern Guangdong province (Zhang et al., 2015b; Liu et al., 2017a, b; Qiu et al., 2017a, b; Yan et al., 2017; Jia et al., 2018, 2020; Zhou et al., 2018; Supplementary Table 5). In addition, several I-, S-, or A-type granites are found in central, northern, and southern Guangdong province (Li et al., 2007; Zhu et al., 2010; Huang et al., 2013a; Zhang et al., 2015b; Zheng et al., 2017; Jiang et al., 2018; Liu et al., 2020b, 2021; Supplementary Table 5). Late Mesozoic granites in Guangdong province were emplaced mainly between 193 and 81 Ma, with an age-peak of ca. 160 Ma (Supplementary Fig. 1). In addition to granites, mafic rocks crop out in the northern and coastal areas of Guangdong province (Cao et al., 2009; Zhu et al., 2010; Yan et al., 2017; Jiang et al., 2020; Supplementary Table 5).

Guangzhou area is located in central Guangdong province as well as southeast part of WYO (Fig. 1b and 2). Previous studies have identified Late Ordovician–Early Silurian (446–438 Ma) biotite, muscovite, and two-mica granites in the Baiyunshan–Maofengshan forest park of Guangzhou area (Liu et al., 2020a). Furthermore, Late Jurassic two-mica granites (160–156 Ma), syenite porphyries (162 Ma), and diorites (155 Ma) are exposed in the Huolushan, Longyandong, Maofengshan, and Liupianshan forest parks of Guangzhou area (Guo et al., 2019; Liu et al., 2020b, 2021). In addition to igneous rocks, outcrops of Early Paleozoic and Early Mesozoic sedimentary rocks, Proterozoic metamorphic rocks, and quaternary sediments are found in the Guangzhou area (Fig. 3). This paper reports newly discovered Early Silurian biotite granodiorites and Late Jurassic biotite granites from the Guangzhou area of SE WYO (Fig. 3). The petrographic characteristics of these granites are described below.

Early Silurian biotite granodiorites are dark gray and medium grained (0.5–1.5 mm), and are composed of plagioclase (35–40 vol%), quartz (20–25 vol%), K-feldspar (10–15 vol%), and biotite (10–15 vol %), with minor zircon, apatite, monazite, and Fe–Ti oxides (Fig. 4a, e). They commonly show gneissic banding, with discontinuous biotite foliation (Fig. 4a, e). Late Jurassic biotite granites are gray or pink and show a medium- to coarse-grained inequigranular texture. They are composed of quartz (25–30 vol%), plagioclase (25–30 vol%), K-feldspar (20–25 vol%), and biotite (5–10 vol%), with minor zircon, apatite, and Fe–Ti oxides (Fig. 4b–d, f–h).

3. Results

Analytical methods, including mineral composition analyses, zircon U–Pb age dating, whole-rock major- and trace-element analyses, Sr–Nd isotope analyses, and zircon O and Lu–Hf isotope analyses, are described in Supplementary text 1.

3.1. Zircon U–Pb ages

Laser ablation–inductively coupled plasma–mass spectrometry (LA–ICP–MS) zircon U–Pb dating results for the biotite granodiorite and biotite granites are compiled in Supplementary Table 1 and presented in Fig. 5. Most zircon grains from the biotite granodiorite and biotite granites have sizes of 100–250 μm with aspect ratios of 2:1 to 3:1. Zircon grains from the biotite granodiorite and biotite granites display oscillatory zoning in cathodoluminescence (CL) images (Fig. 5a–e). The clearly zoned or homogeneous textures and high Th/U ratios (0.05–1.61) of zircon grains from the biotite granodiorite and biotite granites indicate a magmatic origin (Hoskin and Black, 2000).

LA–ICP–MS zircon U–Pb dating of biotite granodiorite sample 17GZ08-1 yielded $^{206}Pb/^{238}U$ ages of 456–434 Ma with a weighted-mean age of 441.7 ± 1.6 Ma (2σ; MSWD = 0.77; n = 17) (Fig. 5a; Supplementary Table 1). In addition, LA–ICP–MS zircon U–Pb dating of biotite granite samples 17GZ02-1, 17GZ07-1, 17GZ08-2, and 17GZ10-1 yielded $^{206}Pb/^{238}U$ ages of 165–151 Ma, 168–160 Ma, 164–152 Ma, and 169–159 Ma, respectively, with weighted-mean ages of 159.1 ± 0.6 Ma (2σ; MSWD = 1.6; n = 19), 163.6 ± 0.5 Ma (2σ; MSWD = 0.6; n = 23), 158.9 ± 1.3 Ma (2σ; MSWD = 0.07; n = 22), and 162.5 ± 0.6 Ma (2σ; MSWD = 0.53; n = 22), respectively (Fig. 5b–e; Supplementary Table 1).

3.2. Mineral compositions

Mineral composition data for the biotite granodiorites and biotite granites are given in Supplementary Table 2. Plagioclases in the Early Silurian biotite granodiorites are andesine and oligoclase ($An_{24–37}Ab_{61–75}Or_{0–3}$) (Fig. 6a). In the Late Jurassic biotite granites, plagioclases are also andesine and oligoclase ($An_{13–46}Ab_{52–86}Or_{1–3}$), and K-feldspars are all sanidine ($An_{0–1}Ab_{4–32}Or_{67–96}$) (Fig. 6a). Biotites in the Early Silurian biotite granodiorites and Late Jurassic biotite granites are classified as lepidomelane, with FeO contents of 22.3–24.5 wt% and 21.0–24.9 wt%, MgO contents of 5.6–7.1 wt% and 6.6–9.0 wt%, and TiO_2 contents of 2.6–3.3 wt% and 1.8–4.2 wt%, respectively (Fig. 6b).

3.3. Whole-rock major and trace elements

3.3.1. Early Silurian biotite granodiorites

Whole-rock major- and trace-element data for the studied biotite granodiorites are given in Supplementary Table 3. Early Silurian biotite granodiorite samples have SiO_2, K_2O, and Na_2O contents of 67.8–69.4 wt%, 1.7–2.8 wt%, and 3.1–3.4 wt%, respectively. The samples plot in the medium-K or subalkalic fields in discrimination diagrams (Fig. 7a–b, d). They have consistent A/CNK (molar $Al_2O_3/[CaO + Na_2O + K_2O]$) values of 1.13 and plot in the strongly peraluminous field with $Mg^{\#}$ (molar MgO/[molar MgO + molar FeO^T] × 100; assuming $FeO^T = 0.90 \times Fe_2O_3^T$) values of 33.4–36.0 (Fig. 7c; Supplementary Table 3).

Early Silurian biotite granodiorites show enrichment in light rare-earth elements (LREEs), moderately fractionated REE patterns ($(La/Sm)_{CN}$ = 4.3–4.4, where "CN" denotes chondrite-normalized), and moderate negative Eu anomalies ($Eu/Eu^* = Eu_{CN}/(Sm_{CN} \times Gd_{CN})^{1/2}$) of 0.42–0.55 in a chondrite-normalized element-variation diagram (Fig. 8a). In a primitive-mantle (PM)-normalized element-variation diagram, the Early Silurian biotite granodiorites display enrichment in Rb, Th, U, and Pb and show negative Ba, Sr, Nb, and Ti anomalies (Fig. 8b). REE and trace-element compositions of these two Early Silurian biotite granodiorites overlap with those of Late Ordovician–Early Silurian (biotite, two-mica, and muscovite) granites from the Baiyunshan and Maofengshan forest parks of Guangzhou area, SE WYO (Liu et al., 2020a; Fig. 8a–b).

3.3.2. Late Jurassic biotite granites

Late Jurassic biotite granites have SiO_2 contents of 68.2–72.6 wt%, K_2O contents of 3.8–6.6 wt%, and Na_2O contents of 2.5–3.1 wt%, with $K_2O > Na_2O$, and plot in the shoshonitic or subalkalic fields in discrimination diagrams (Fig. 7a–b, d; Supplementary Table 3). Their A/CNK values range from 1.01 to 1.06 and plot in the weakly peraluminous field with $Mg^{\#}$ values of 30.7–36.3 (Fig. 7c; Supplementary Table 3).

Late Jurassic biotite granites are moderately to significantly enriched in LREEs [$(La/Sm)_{CN}$ = 3.7–8.3; Fig. 8c]. These granites show slight to

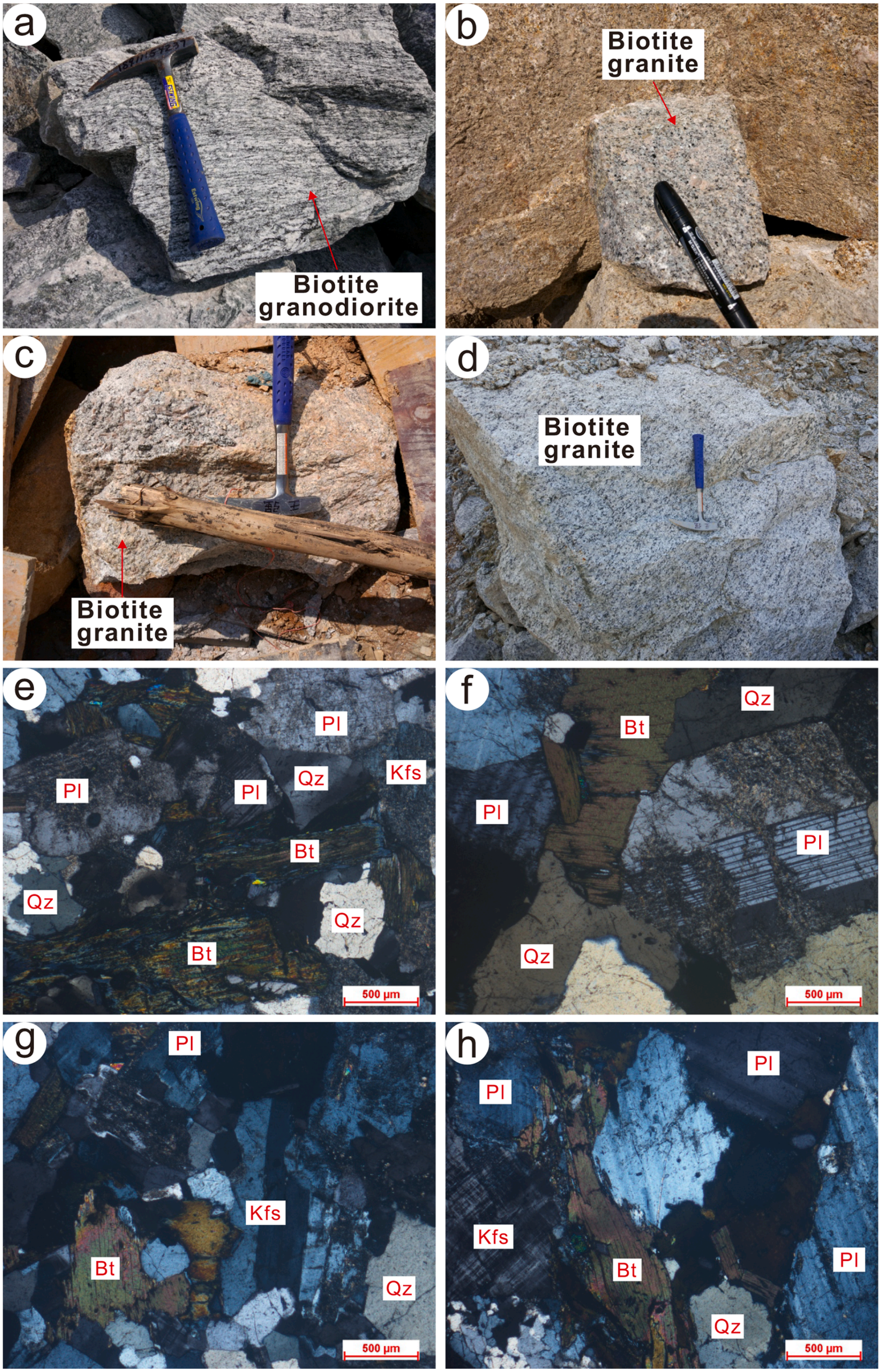

Fig. 4. Field photographs and photomicrographs of Early Silurian granodiorites and Late Jurassic biotite granites in the Guangzhou area of SE WYO. (a, e) Early Silurian biotite granodiorites; (b–d, f–h) Late Jurassic biotite granites. (e–h) were taken under cross-polarized light. Mineral abbreviations: Bt: biotite, Kfs: K-feldspar, Pl: plagioclase, Qz: quartz (after Whitney and Evans, 2010).

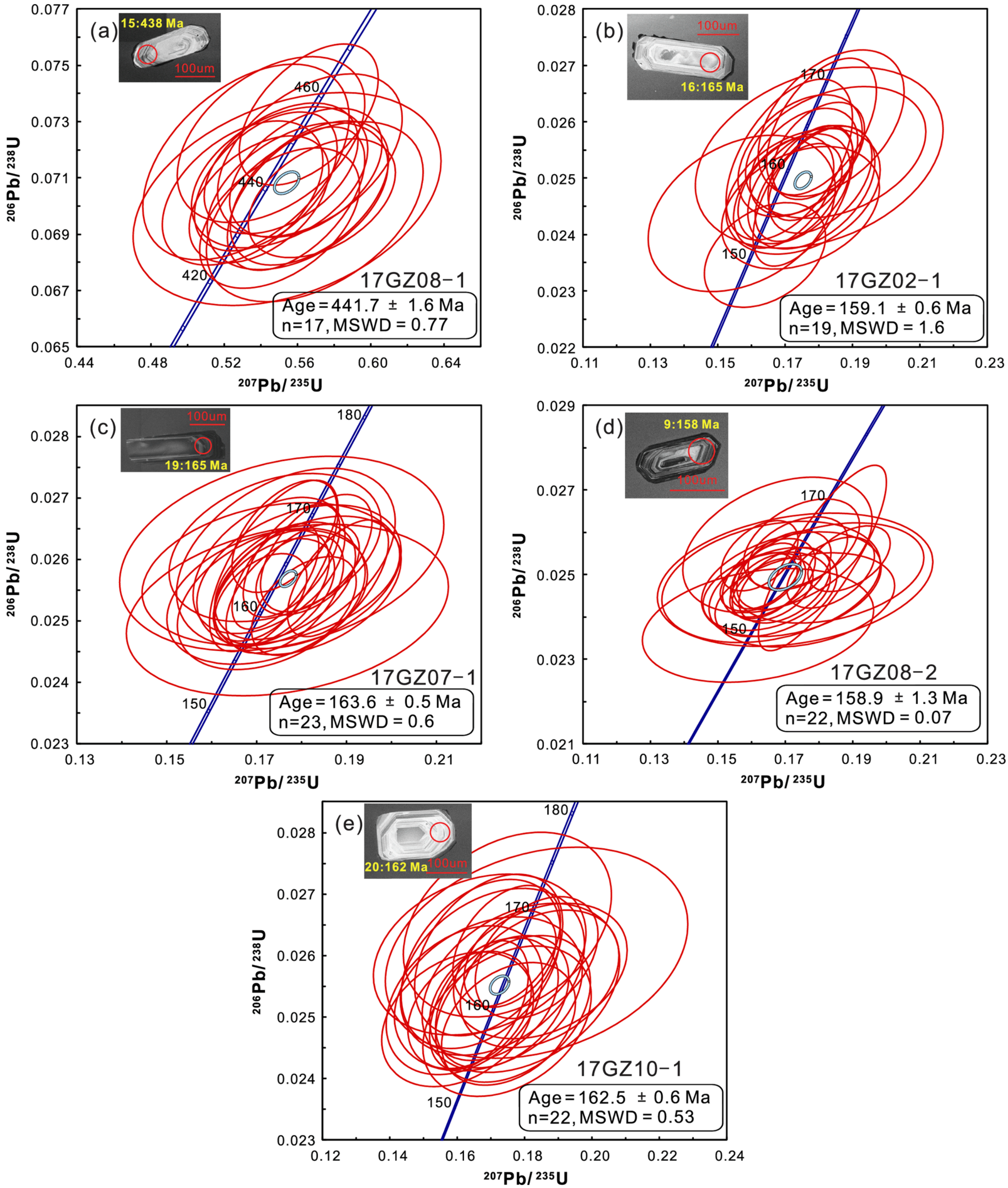

Fig. 5. LA–ICP–MS zircon U–Pb concordia diagrams and CL images of Early Silurian biotite granodiorite (a, 17GZ08-1) and Late Jurassic (b, 17GZ02-1; c, 17GZ07-1; d, 17GZ08-2; and e, 17GZ10-1) biotite granites in the Guangzhou area of SE WYO. Red circles on the CL images of zircon grains are LA–ICP–MS analysis locations. Yellow numbers are ages. (For interpretation of the references to colour in this figure legend, the reader is referred to the web version of this article.)

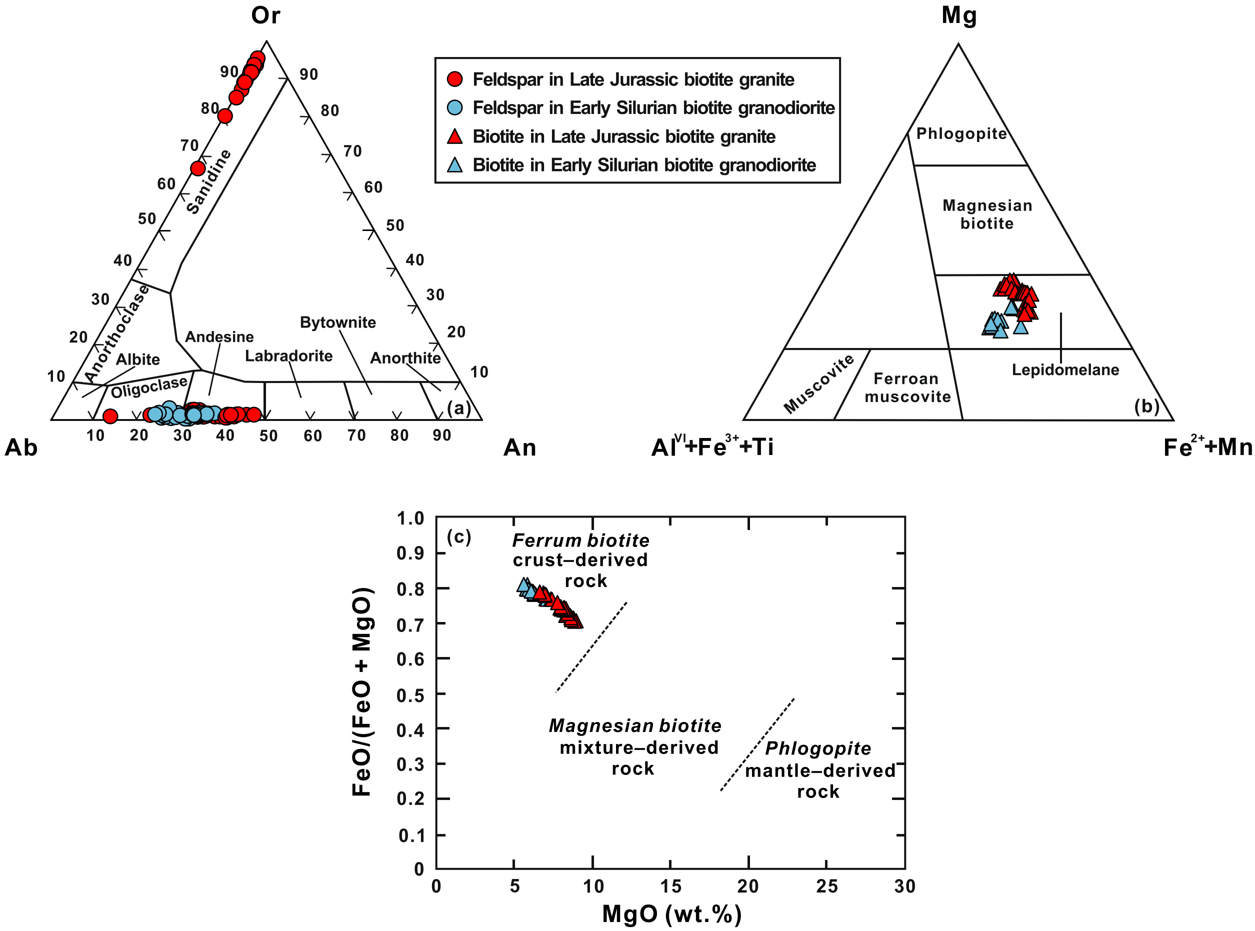

Fig. 6. Mineral compositions of Early Silurian biotite granodiorites and Late Jurassic biotite granites in the Guangzhou area of SE WYO. (a) Feldspar Ab–Or–An diagram. Ab: albite, Or: K-feldspar, An: anorthite. (b) Mica compositions plotted in a ternary Mg–(Al^{VI} + Fe^{3+} + Ti)–(Fe^{2+} + Mn) diagram. (c) FeO/(FeO + MgO) versus MgO diagram for biotite (after Xia et al., 2014).

pronounced negative Eu anomalies (Eu/Eu* = 0.24–0.74) except for one sample (17GZ11-1) that exhibits slight positive Eu anomalies (Eu/Eu* = 1.2; Fig. 8c). In a PM-normalized element-variation diagram, Late Jurassic biotite granites display enrichment in Rb, Th, U, and Pb and show negative Ba, Sr, Nb, Ta, and Ti anomalies (Fig. 8d). REE and trace-element compositions of these Late Jurassic biotite granites are overall similar to those of Late Jurassic two-mica granites in the Huolushan, Longyandong, and Maofengshan forest parks of Guangzhou area, SE WYO (Liu et al., 2020b, 2021; Fig. 8c).

3.4. Sr–Nd–Hf–O isotopic compositions

3.4.1. Early Silurian biotite granodiorites

Whole-rock Sr–Nd and zircon Hf–O isotope data for Early Silurian biotite granodiorites and Late Jurassic biotite granites are given in Supplementary Tables 3–4. Initial Sr–Nd–Hf isotopic ratios were calculated according to the obtained LA–ICP–MS zircon U–Pb ages for Early Silurian biotite granodiorite (442 Ma) and Late Jurassic biotite granites (164–159 Ma), respectively. Early Silurian biotite granodiorites have enriched Nd isotopic compositions ($\varepsilon_{Nd}(t) = -7.8$ to -7.6), with two-stage Nd model ages ranging from 1.82 to 1.81 Ga (Fig. 9b; Supplementary Table 3). As Early Silurian biotite granodiorites have relatively high $^{87}Rb/^{86}Sr$ ratios (6.8 to 8.5 > 2.0; Supplementary Table 3), we did not calculate their initial $^{87}Sr/^{86}Sr$ ratios. Zircon grains in Early Silurian biotite granodiorite sample 17GZ08-1 have variable initial $^{176}Hf/^{177}Hf$ ratios (0.2822–0.2824) and $\varepsilon_{Hf}(t)$ values (−10.3 to − 1.7), with two-stage Hf model ages ranging from 2.1 to 1.5 Ga (Fig. 9c and 10; Supplementary Table 4). Zircon grains in 17GZ08-1 have homogeneous $\delta^{18}O$ values between 8.6‰ and 9.3‰ (Fig. 10; Supplementary Table 4). Early Silurian biotite granodiorites also have similar Nd–Hf–O isotopic compositions to those of Late Ordovician–Early Silurian (biotite, two-mica, and muscovite) granites in the Baiyunshan and Maofengshan forest parks of Guangzhou area, SE WYO (Figs. 9 and 10; $\varepsilon_{Nd}(t) = -12.1$ to -7.6; $\varepsilon_{Hf}(t) = -11.4$ to -0.8; $\delta^{18}O$ = 8.5‰–10.0‰; Liu et al., 2020a).

3.4.2. Late Jurassic biotite granites

Late Jurassic biotite granites have variable initial $^{87}Sr/^{86}Sr$ ratios (0.7108–0.7210), $\varepsilon_{Nd}(t)$ values (−11.7 to − 8.1), initial $^{176}Hf/^{177}Hf$ ratios (0.2822–0.2825), $\varepsilon_{Hf}(t)$ values (−17.2 to − 6.2), and $\delta^{18}O$ values (7.4‰–10.6‰) (Figs. 9 and 10; Supplementary Tables 3–4). Their two-stage Nd and Hf model ages range from 1.9 to 1.6 Ga and from 2.3 to 1.6 Ga, respectively (Supplementary Tables 3–4). Late Jurassic biotite granites have similar Sr–Nd–Hf–O isotopic compositions to those of Late Jurassic two-mica granites in the Huolushan, Longyandong, and Maofengshan forest parks of Guangzhou area, SE WYO (Figs. 9 and 10; $^{87}Sr/^{86}Sr$ = 0.7094–0.7145; $\varepsilon_{Nd}(t) = -10.5$ to -9.3; $\varepsilon_{Hf}(t) = -14.2$ to -4.2; $\delta^{18}O$ = 6.8‰–10.4‰; Liu et al., 2020b, 2021).

4. Discussion

4.1. Petrogenesis

4.1.1. Early Silurian biotite granodiorite

Whole-rock $Mg^{\#}$ values (33.4–36.0) and Nd isotopic compositions ($\varepsilon_{Nd}(t) = -7.8$ to -7.6) and zircon Hf-O isotopic compositions ($\varepsilon_{Hf}(t)$

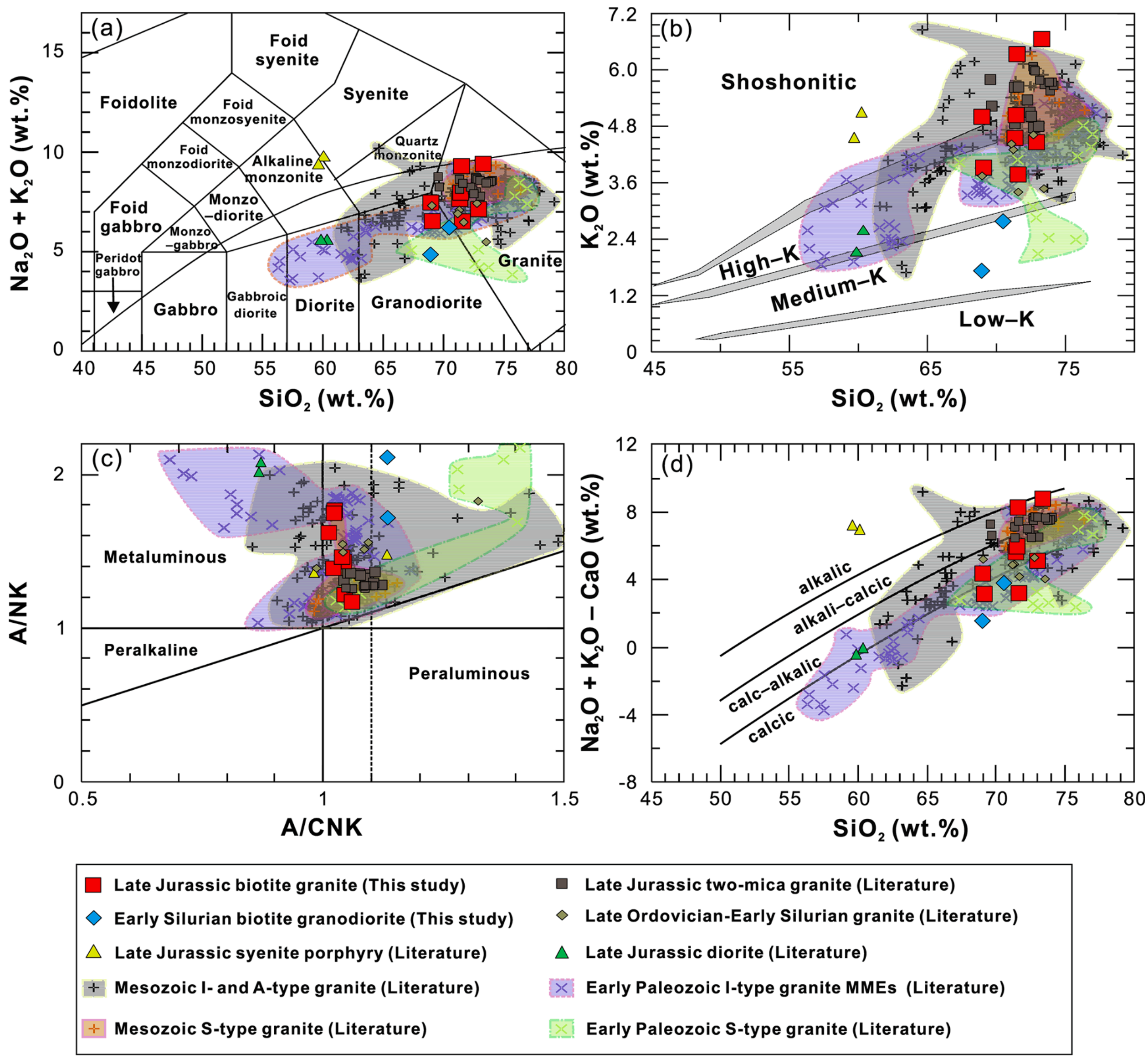

Fig. 7. Major-element classification diagrams for Early Silurian biotite granodiorites and Late Jurassic biotite granites in the Guangzhou area of SE WYO: (a) Total-alkali–silica (TAS) diagram; (b) K_2O versus SiO_2 diagram; (c) A/NK versus A/CNK diagram; A/NK = molar $Al_2O_3/(Na_2O + K_2O)$, A/CNK = molar $Al_2O_3/(CaO + Na_2O + K_2O)$; (d) ($Na_2O + K_2O - CaO$) versus SiO_2 diagram. Data for Late Ordovician–Early Silurian granites from the Guangzhou area of SE WYO are from Liu et al. (2020a); data for Late Jurassic two-mica granites, syenite porphyries, and diorites from the same area are from Liu et al. (2020b, 2021); data for Early Paleozoic I-type granites and mafic microgranular enclaves (MMEs) within them and S-type granites and Mesozoic I-, S-, and A-type granites from Guangdong province of southern Nanling Range are from references compiled in Supplementary Table 5.

= − 10.3 to − 1.7, $\delta^{18}O$ = 8.6‰-9.3‰) suggest that the magma source material of Early Silurian biotite granodiorites was Paleoproterozoic crustal rocks of the Cathaysia Block. Whole-rock $Mg^{\#}$ values of Early Silurian biotite granodiorites are similar to those of pure crustal (metaigneous and metasedimentary rocks) partial melts that have been determined in experimental studies (Supplementary Fig. 2; Patiño Douce and Johnston, 1991; Patiño Douce and Beard, 1995). In addition, biotites of Early Silurian biotite granodiorites are Fe-rich biotites that crystallized from pure-crust-derived magmas (Xia et al., 2014; Fig. 6b and c). Moreover, in an $\varepsilon_{Nd}(t)$ versus age diagram, Early Silurian biotite granodiorites fall within the field of the Longquan–Mayuan groups in basement of the Cathaysia Block with two-stage Nd model age of 1.8 Ga (Fig. 9b; Supplementary Table 3). Furthermore, zircon Hf-O isotopic compositions of Early Silurian biotite granodiorites are different from mantle-derived Qinghu syenites (Fig. 10). Therefore, it is inferred that Early Silurian biotite granodiorites were derived from partial melting of basement Paleoproterozoic crustal rocks of the Cathaysia Block.

The A/CNK values > 1.1 and K_2O/Na_2O ratios < 1.0 further indicate that the magma source of Early Silurian biotite granodiorites was amphibolites. In general, granitic rocks with A/CNK values > 1.1 could be formed by partial melting of metasedimentary rocks (Patiño Douce, 1999) or by hydrous melting of metaluminous basaltic to andesitic rocks (Beard and Lofgren, 1991; Patiño Douce and Beard, 1995; Sisson et al., 2005). Metasedimentary rocks-derived granitic melts are characterized by K_2O/Na_2O ratios > 1.0 (Chappell and White, 2001), which are inconsistent with K_2O/Na_2O ratios < 1.0 of Early Silurian biotite granodiorites (0.56–0.82; Supplementary Table 3). In addition, Early Silurian biotite granodiorites also have higher MgO contents (1.0–1.5 wt %) than metasedimentary rocks-dominated crustal source-derived Late Jurassic biotites (0.46–0.99 wt%; Supplementary Table 3; discussed below). Therefore, Early Silurian biotite granodiorites were possibly derived from *meta*-igneous source. The metamorphic basement of the eastern SCB consists of paragneiss, migmatite, schist, and amphibolite (Zhang et al., 2012, and references therein). Therefore, we suggest that

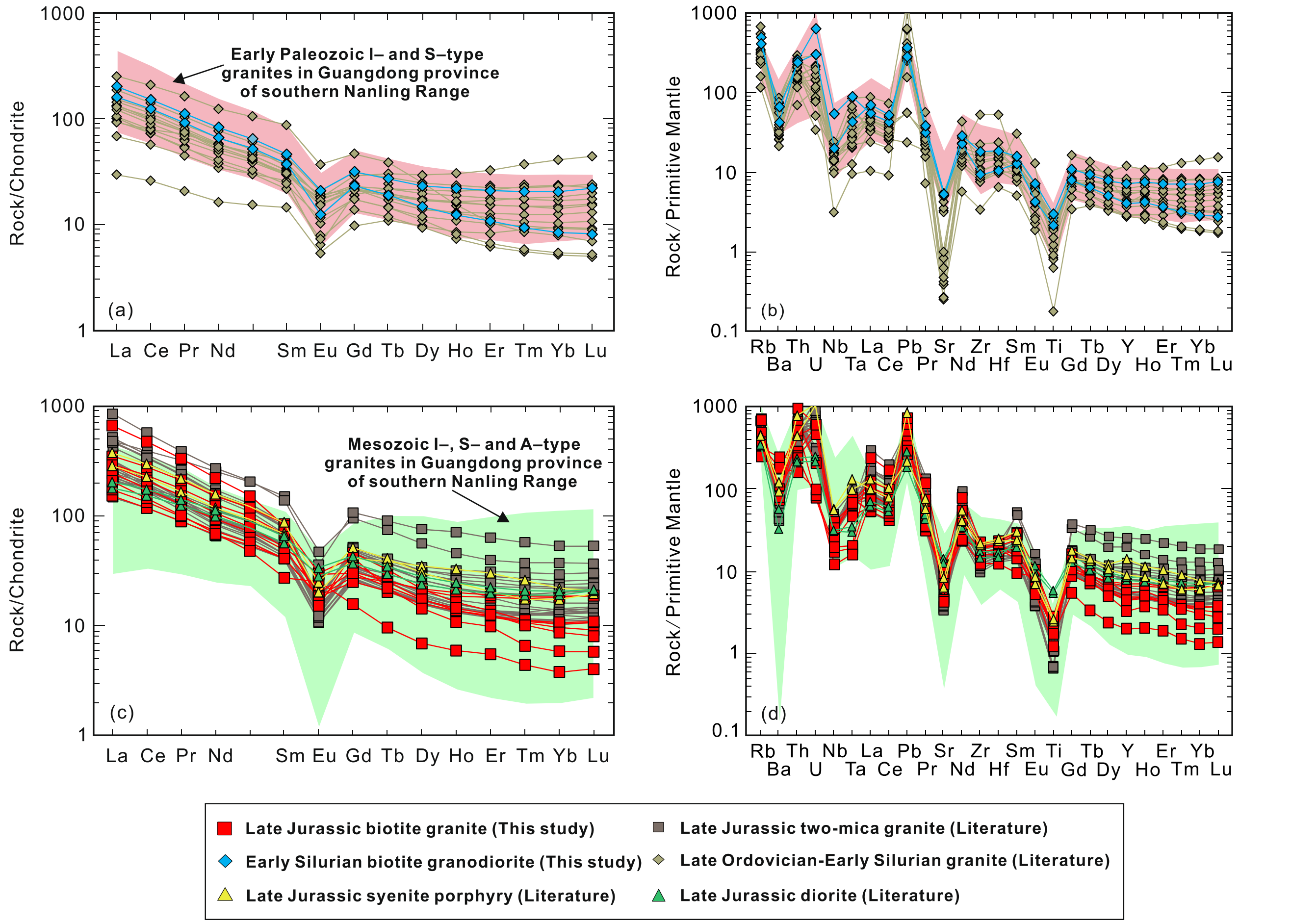

Fig. 8. (a, c) Chondrite-normalized REE patterns and (b, d) primitive-mantle-normalized multi-element diagram for Early Silurian biotite granodiorites and Late Jurassic biotite granites, respectively in the Guangzhou area of SE WYO. Normalizing values are from Sun and McDonough (1989). Data sources are the same as in Fig. 7.

magma source *meta*-igneous rocks of Early Silurian biotite granodiorites were amphibolites. Similar examples of peraluminous I-type granites also include Lachlan granites from the southeastern Australia (Chappell et al., 2012) and Gangdese granites in the southern Tibet (Ma et al., 2017).

Experimental studies have shown that hydrous melting of amphibolites can generate a strongly peraluminous melt, while dehydration melting of amphibolites yield weakly peraluminous granodioritic melts (Beard and Lofgren, 1991). In addition, temperature of dehydration melting of amphibolites is higher than 850 °C (Beard and Lofgren, 1991). Strongly peraluminous compositions (A/CNK = 1.13; Fig. 7c) and zircon and monazite saturation temperatures lower than 850 °C (T_{Zr} = 757–812 °C and T_{LREE} = 761–778 °C, respectively; Supplementary Fig. 3) of Early Silurian biotite granodiorites support that they were possibly generated by hydrous melting of amphibolites. The external fluids could have been migrated along one of the many regional shear zones, such as the Heyuan-Shaowu shear zone in Guangdong Province, or via the advection of regional metamorphic fluids (Yu et al., 2019, and references therein).

The magma that formed Early Silurian biotite granodiorites may have originated from a depth of > 30 km (lower crust), as inferred from their La/Yb and Sr/Y ratios. La/Yb and Sr/Y ratios of felsic rocks intrinsically reflect the presence of mineral assemblages in the magma source region (Tang et al., 2017, and references therein). In an Sr/Y versus La/Yb diagram, Early Silurian biotite granodiorites plot within the stability field of plagioclase and garnet (La/Yb = 13.9–26.7, Sr/Y = 3.4–5.8;Supplementary Fig. 4). Given that garnet can be stable to pressures as low as 9.0 kbar (corresponding to a crustal depth of 30 km) during partial melting of mafic metamorphic rocks (Zhao et al., 2007, and references therein), the magma origin depth of Early Silurian biotite granodiorites is > 30 km (assuming a pressure gradient of 0.3 kbar/km).

4.1.2. Late Jurassic biotite granite

4.1.2.1. Hybridized magma source. Low whole-rock Mg# values (30.7–36.3) and enriched whole-rock Nd and zircon Hf isotopic compositions ($\varepsilon_{Nd}(t) = -11.7$ to -8.1, $T_{2DM} = 1.9$–1.6 Ga; $\varepsilon_{Hf}(t) = -17.2$ to -6.2, $T_{2DM} = 2.3$–1.6 Ga) also suggest that the magma source material of Late Jurassic biotite granites comprised Paleoproterozoic crustal rocks of the Cathaysia Block. Similar to those of Early Silurian biotite granodiorites, whole-rock Mg# values of Late Jurassic biotite granites plot in the field of pure crustal partial melts as determined in experimental studies (Supplementary Fig. 2). In addition, Late Jurassic biotite granites exhibit similar whole-rock Nd isotopic compositions to those of basement of the Cathaysia Block (Fig. 9b). Moreover, zircon Hf isotopic compositions of Late Jurassic biotite granites are similar to those of ancient-crust-derived Early Cretaceous volcanic rocks of the Cathaysia Block ($\varepsilon_{Hf}(t) = -12.8$ to -7.5, $T_{2DM} = 2.0$–1.7 Ga; Liu et al., 2012).

The similar whole-rock Th contents and Th/La ratios to those of metasedimentary-derived granites, weakly peraluminous compositions (A/CNK = 1.01–1.06), and the wide range of zircon O isotopic compositions ($\delta^{18}O$ = 7.4‰–7.9‰) of Late Jurassic granites suggest they were derived from a hybridized source dominated by metasedimentary rocks

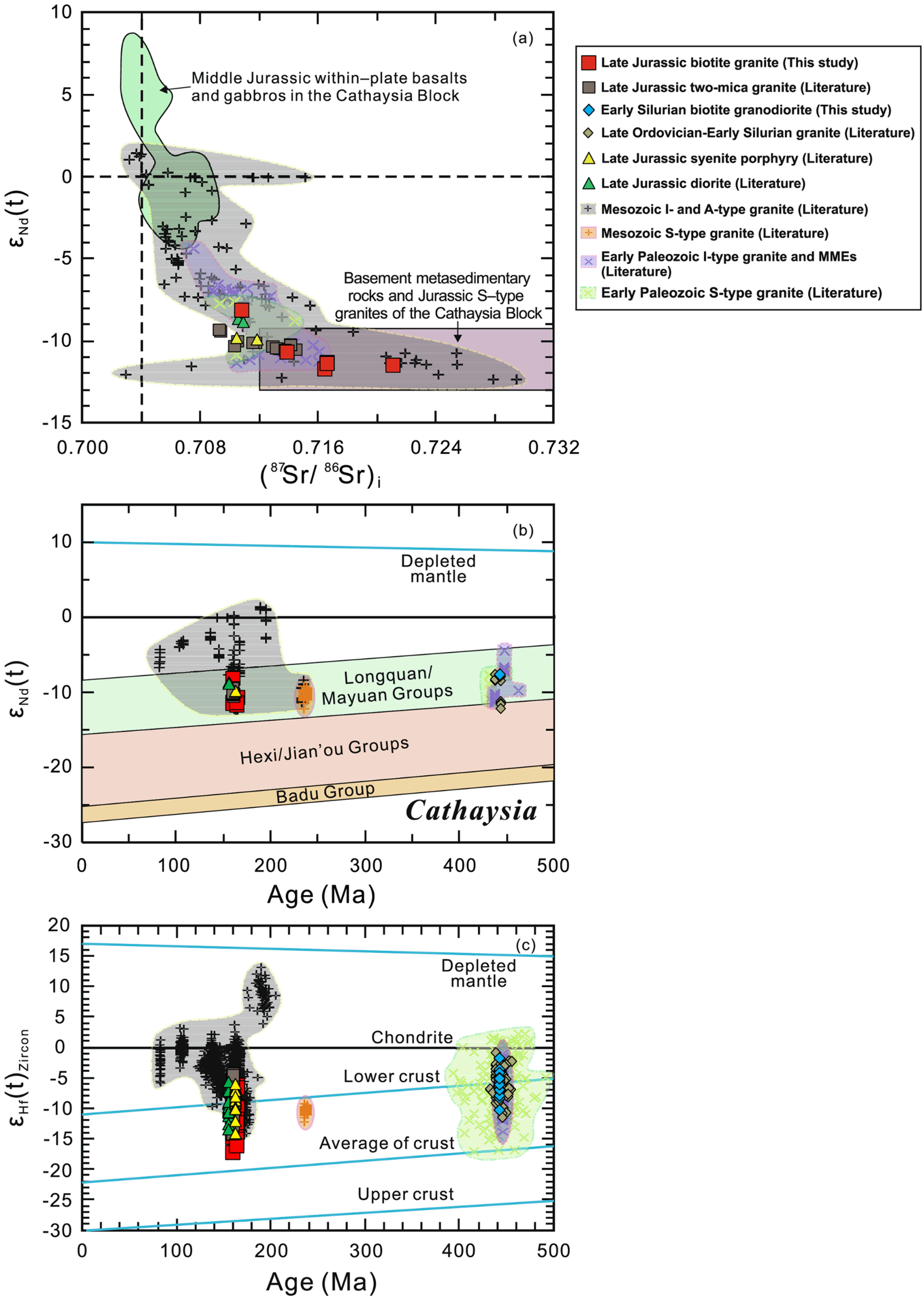

Fig. 9. (a) $\varepsilon_{Nd}(t)$ versus $(^{87}Sr/^{86}Sr)_i$ diagram for Late Jurassic biotite granites in the Guangzhou area of SE WYO. Data for Middle Jurassic within-plate basalts and gabbros of the Cathaysia Block are from Li et al. (2003) and Wang et al. (2003), and data for basement metasedimentary rocks and Jurassic S-type granites of the Cathaysia Block are from Yuan et al. (1991), Shen et al. (1999), and Jiang and Zhu (2017). Initial Sr–Nd isotopic compositions of basement metasedimentary rocks and Mesozoic S-type granites of the Cathaysia Block are recalculated to 160 Ma. (b) Nd isotopic evolution of the Cathaysia Block (modified from Chen and Jahn, 1998). (c) Zircon $\varepsilon_{Hf}(t)$ versus age diagram for Early Silurian biotite granodiorite and Late Jurassic biotite granites in the Guangzhou area of SE WYO. Data sources are the same as in Fig. 7.

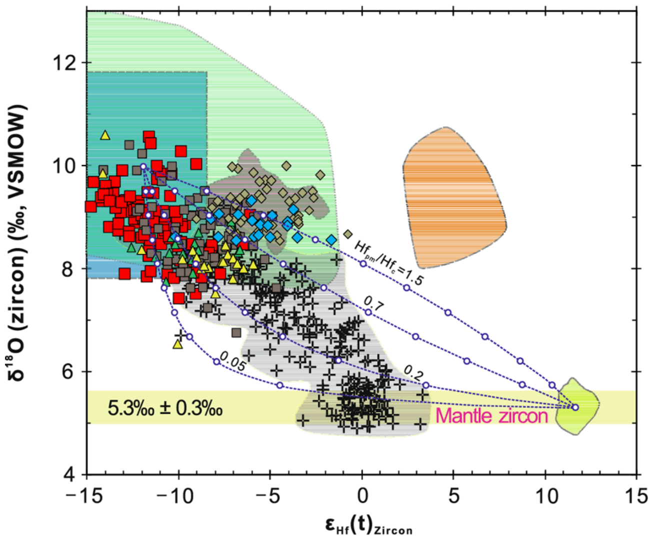

Fig. 10. Zircon Hf versus O isotopic compositions of Early Silurian biotite granodiorites and Late Jurassic biotite granites in the Guangzhou area of SE WYO (modified from Li et al., 2009b). Data sources: Qinghu syenite, Li et al. (2009b); Jiuyishan granite, Huang et al. (2011); Darongshan granite, Jiao et al. (2015); Jiuling granite, Rong et al. (2017); Himalayan leucogranite, Hopkinson et al. (2017). Other data sources are the same as in Fig. 7. The dotted lines denote two-component mixing trends between mantle- and supracrustal-derived magmas. Hf_{pm}/Hf_c is the ratio of the Hf concentration in the parental mantle magma (pm) to crustal melt (c) for each curve, and the small open circles represent 10% mixing increments assuming that mantle zircon has $\varepsilon_{Hf} = +12.0$ and $\delta^{18}O = 5.6‰$ and that supracrustal zircon has $\varepsilon_{Hf} = -12.0$ and $\delta^{18}O = 10.0‰$.

with subordinate juvenile crustal rocks. Whole-rock Th contents and Th/La ratios (13.3–79.3 ppm and 0.27–0.95, respectively) of Late Jurassic biotite granites are similar to those of Late Jurassic two-mica granites from the Guangzhou area of SE WYO as well as metasedimentary-rock-derived Himalayan leucogranites (Th = 1.4–61.8 ppm, Th/La = 0.2–1.9; Guo and Wilson, 2012; Liu et al., 2020b, 2021).

However, experimental studies have suggested that partial melts of metasedimentary rocks (metagraywackes and metapelites) are strongly peraluminous (A/CNK > 1.1) (Patiño Douce and Harris, 1998), which is inconsistent with Late Jurassic biotite granites, which are weakly peraluminous (A/CNK = 1.01–1.06). In addition, several zircons from the Late Jurassic biotite granites also exhibit $\delta^{18}O$ values (7.4‰–7.9‰; Supplementary Table 4) that are lower than those of the above-mentioned metasedimentary-rock-derived granites ($\delta^{18}O$ > 8.0‰; Fig. 10). The negative relationship between zircon $\varepsilon_{Hf}(t)$ and $\delta^{18}O$ (Fig. 10) indicates that metaluminous juvenile crustal rocks or mantle-derived mafic magmas with depleted Hf isotopic compositions and low $\delta^{18}O$ values were involved in the source material of Late Jurassic biotite granites. A simple mass balance calculation is shown on a $\delta^{18}O$ vs $\varepsilon_{Hf}(t)$ diagram (Fig. 10) using the SCB Triassic Darongshan granites (Jiao et al., 2015) as the crustal sediments component and the Qinghu syenites to represent the mantle end-member. The Darongshan granites are typical cordierite-bearing granites with high mean $\delta^{18}O_{zircon}$ of 11.0‰ and low mean $\varepsilon_{Hf}(t)_{zircon}$ of −10.0 and were considered to have been generated by melting of the metasedimentary rocks (Jiao et al., 2015). The Qinghu syenites with mantle-like $\delta^{18}O_{zircon}$ of 5.4 ± 0.3‰ and high $\varepsilon_{Hf}(t)_{zircon}$ of + 11.6 were derived from lithospheric mantle without appreciable crustal contamination (Li et al., 2009b). The modelling results indicate that Late Jurassic biotite granites might contain 20%–50% of PM-derived material (Fig. 10). However, this is inconsistent with the whole-rock radiogenic initial $^{87}Sr/^{86}Sr$ ratios (0.7108–0.7210 > 0.7098) and unradiogenic Nd isotope compositions ($\varepsilon_{Nd}(t) = -11.7$ to -8.1) of Late Jurassic biotite granites. Furthermore, biotites from Late Jurassic biotite granites are Fe-rich biotites that crystallized from pure-crust-derived magmas (Xia et al., 2014; Fig. 6b and c). Therefore, we suggest that other juvenile crustal rocks were involved in the metasedimentary-rock source of Late Jurassic biotite granites. In summary, the source materials of Late Jurassic biotite granites were dominated by metasedimentary rocks with minor juvenile crustal rocks. Other examples that have similar magma source with Late Jurassic biotite granites include the Jiufeng granites in the SCB (Huang et al., 2015) and the Lachlan granites in southeastern Australia (Kemp et al., 2008).

Late Jurassic biotite granites were probably derived by partial melting of metasedimentary rocks, driven by the fluid-absent mica breakdown reaction in the middle-lower crust (>16.5 km). K_2O contents (3.8–6.6 wt%) of Late Jurassic biotite granites are higher than their Na_2O (2.4–3.1 wt%) contents (Supplementary Table 3). In addition, Late Jurassic biotite granites have higher zircon and monazite saturation temperatures (T_{Zr} = 769–819 °C and T_{LREE} = 740–846 °C, respectively; Supplementary Fig. 3) relative to the temperature of water-fluxed melting (~700 °C; Sawyer et al., 2011). In a Sr/Y versus La/Yb diagram, most of the Late Jurassic biotite granites plot within the stability field of plagioclase and garnet (La/Yb = 11.7–163, Sr/Y = 3.6–26.3; Supplementary Fig. 4). Given that garnet can be stable to pressures as low as 5 kbar (corresponding to a crustal depth of 16.5 km) during partial melting of metasedimentary rocks (Patiño Douce and Harris, 1998), the magma origin depth of Late Jurassic biotite granites is > 16.5 km (assuming a pressure gradient of 0.3 kbar/km). Three Late Jurassic biotite granite samples (17GZ10-1, 17GZ10-2, and 17GZ11-1) that were collected from the same plutonic rock near Yonghe town of Guangzhou area (Fig. 3) show higher La/Yb (47.2–163) and Sr/Y (12.3–26.3) ratios compared with the other Late Jurassic biotite granites (La/Yb = 11.7–46.0 and Sr/Y = 3.6–7.4) (Supplementary Fig. 4). In addition, these three samples exhibit moderate negative to slight positive Eu anomalies (Eu/Eu* = 0.5–1.2), which differ from those of other Late Jurassic biotite granites that have moderate to pronounced negative Eu anomalies (Eu/Eu* = 0.2–0.6; Fig. 8c). We suggest that these characteristics may have resulted from a higher amount of garnet but lower amount of plagioclase in the residual source of these three samples relative to the other Late Jurassic biotite granite samples.

4.1.2.2. Fractional crystallization. Late Jurassic biotite granites may have undergone fractional crystallization of biotites and plagioclases based on the following lines of evidence. In a Harker diagram, the gradual decreases in TiO_2, $Fe_2O_3^T$ and MgO contents with increasing SiO_2 contents reflect separation of biotites (Supplementary Fig. 5). In addition, the gradual decreases in Al_2O_3 and CaO contents with increasing SiO_2 contents (Supplementary Fig. 5) indicate separation of plagioclases, which are enriched in these elements.

4.2. Implications for crustal reworking and geodynamic processes in the SCB

4.2.1. Early Paleozoic

Regional geological and geochemical evidence, as presented below, suggest that the Early Silurian biotite granodiorites were likely formed in an intracontinental orogenic belt. In general, mafic magmas that were derived from mantle wedges newly metasomatized by slab-derived fluid or melt are marked by positive $\varepsilon_{Nd}(t)$ values. However, early Paleozoic mafic intrusive and volcanic rocks in the SCB have enriched $\varepsilon_{Nd}(t)$ values (-8.9 to −0.6; Yao et al., 2012; Wang et al., 2013c; Zhong et al., 2014, 2016; Zhang et al., 2015a). They were originated from lithospheric mantle that was metasomatized by slab- and sediment-derived melts plus fluid fluxing from the Earliest Neoproterozoic oceanic subduction rather than Paleozoic subduction (Wang et al., 2013c). In addition, magmatic rocks that were formed in subduction zone generally show younging trends with roll-back of the slab (Li and Li, 2007) or forward migration of the frontal arc (Yang et al., 2021). However, the Early Paleozoic granites in the SCB generally do not show younging trends from east (coastal provinces) to west (Xuefeng) or from south (Yunkai) to north (Jiangnan) (Fig. 1b). Moreover, the lack of SSZ-type ophiolites, high-pressure–low-temperature metamorphic rocks, and deep-sea turbidites in the SCB suggest that there was no oceanic subduction zone there during the Early Paleozoic (Wang et al., 2011; Shu et al., 2015, 2018). Furthermore, the coherent biostratigraphy and paleoecology (Chen et al., 2010), continuous sedimentary facies, and similar detrital zircon ages (Wang et al., 2011) through the Cathaysia and Yangtze Blocks during the Early Paleozoic also suggest that no open ocean basin existed between these two blocks at that time. Early Paleozoic SCB intracontinental orogenesis may have been driven by geodynamic processes resulting from the amalgamation of the Australian Plate, Indian Plate, and SCB along the northern margin of east Gondwanaland (Wang et al., 2011).

Early Paleozoic magmatic rocks in the SCB are dominated by gneissic and massive granites (Wang et al., 2011; Zhang et al., 2012; Shu et al., 2018). These gneissic and massive granites were formed by partial melting of metasedimentary and metaigneous rocks without obvious addition of juvenile crustal rocks-derived or mantle-derived magmas in response to double-thickening of crust (Fig. 11a; Wang et al., 2011; Shu et al., 2015). Late Ordovician to Early Silurian granitoids in the Guangzhou area of SE WYO display enriched whole-rock Nd and zircon Hf isotopic compositions and high zircon O isotope values ($\varepsilon_{Nd}(t) = -12.1$ to -7.6, $\varepsilon_{Hf}(t) = -11.4$ to -0.8, $\delta^{18}O = 8.5‰–10.0‰$; Liu et al., 2020a; this study). These granitoids were derived mainly from partial melting of ancient metasedimentary rocks or amphibolites (Liu et al., 2020a; this study). Therefore, the Guangzhou area of SE WYO underwent middle- to lower-crustal reworking in response to double-thickening of crust during the Late Ordovician to Early Silurian (Fig. 11a).

However, in addition to pure crustal rock-derived granitoids, various other rocks that were formed by crust-mantle interaction are found in the SCB. These rocks include I-type granites that contain mafic magmatic enclaves (Yu et al., 2018; Xie et al., 2020), A-type granites (Feng et al., 2014; Cai et al., 2017; Xin et al., 2020), basalts–andesites–dacites (Yao et al., 2012), and ultramafic, mafic and intermediate intrusive rocks (Wang et al., 2013c; Zhong et al., 2014, 2016; Supplementary Table 5). These I-type granites, basalts–andesites–dacites, and ultramafic, mafic and intermediate intrusive rocks are slightly younger (441–415 Ma) than pure crustal rock-derived granitoids (460–435 Ma; this study; Wang et al., 2013b; Zhang et al., 2015a; Liu et al., 2020a) and were formed during the orogenic collapse stage of SCB intracontinental orogeny (Yao et al., 2012; Huang et al., 2013b; Wang et al., 2013c; Xie et al., 2020; Fig. 11b). Moreover, Early Devonian (415–400 Ma) A-type granites in central Jiangxi and Fujian provinces and Wuyishan area were formed by partial melting of pre-Cambrian granulitic crustal rocks during the post-orogenic lithospheric extension stage of SCB intracontinental orogeny (Feng et al., 2014; Cai et al., 2017; Xin et al., 2020). In summary, Early Paleozoic intracontinental reworking of the SCB can be divided into three stages, namely, double-thickening of crust, orogenic collapse, and post-orogenic extension from the Middle–Late Ordovician to Early Devonian on the basis of regional geological data (Fig. 11a and b). During the Early Paleozoic, the Guangzhou area of SE WYO underwent

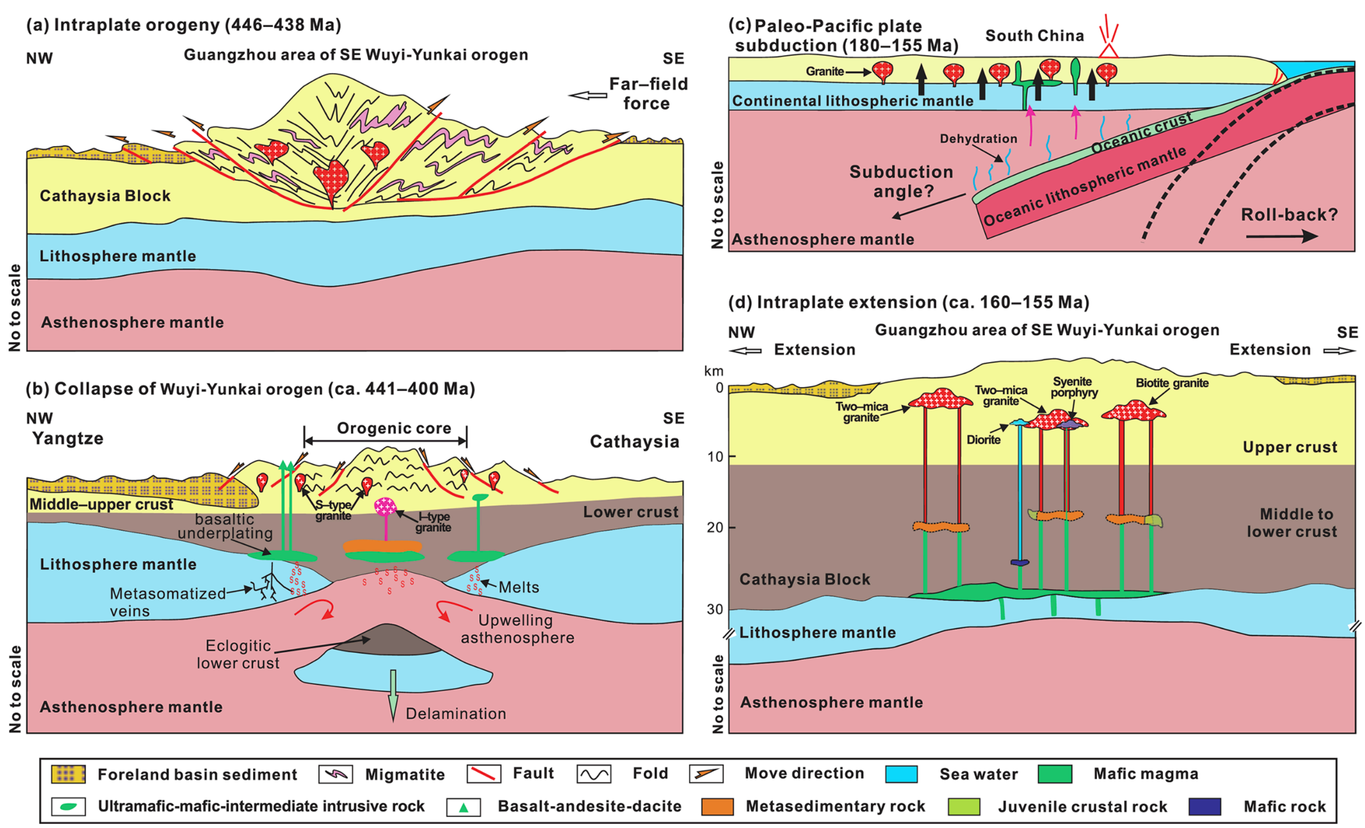

Fig. 11. A petrogenic model for Early Silurian biotite granodiorites and Late Jurassic biotite granites in the Guangzhou area of SE WYO. (a) During the Early Paleozoic, intraplate subduction or overthrusting resulted in crust doubly thickened. The Early Silurian biotite granodiorites were generated by fluid-present hydrous melting of Cathaysia Block basement amphibolites (after Liu et al., 2020a, and references therein). (b) During the Early Silurian–Early Devonian (442–400 Ma), post-orogenic collapse induced asthenospheric upwelling and basaltic magma underplating. (c) Subduction of Paleo-Pacific plate caused mantle-derived mafic magmas underplating in the SCB (after Zhou and Li, 2000; Li and Li, 2007; Jiang et al., 2009, 2015). (d) Heat from mafic magmas caused the partial melting of overlying metasedimentary rocks and juvenile crustal rocks, generating Late Jurassic biotite granites in the Guangzhou area of SE WYO (after Liu et al., 2020b, and references therein).

double-thickening of crust (Late Ordovician to Early Silurian) but without subsequent orogenic collapse and post-orogenic lithospheric extension (Fig. 11a).

4.2.2. Late Mesozoic

Late Mesozoic continental reworking of the SCB was related with flat or oblique subduction of the Paleo-Pacific plate (Zhou and Li, 2000; Li and Li, 2007; Jiang et al., 2009) or intraplate extension/rifting (Wang et al., 2003). Post-orogenic lithospheric extension model could explain transition of magma source of mafic rocks from EMI and EMII (Middle Jurassic-Early Cretaceous) to OIB (Late Cretaceous) (Wang et al., 2003). However, Late Mesozoic granitic magmatism is distributed from inland to coastal region of the SCB (Fig. 2). It is difficult to picture a scenario that the Indosinian movement could propagate into the coastal area. Therefore, there is a general consensus that emplacement of the Mesozoic granites in Cathaysia Block was related to the subduction of the Paleo-Pacific oceanic plate. Flat-slab subduction model is not consistent with newly reported age of Triassic granites. The SCB Triassic granites do not show a younging trend from coast area towards continental interior with more and more geochronological data were reported (Sun et al., 2011, and references therein; Mao et al., 2013a,b, and references therein). In addition, in flat-slab subduction model, the first A-type granite appeared at ca. 190 Ma in hinterland of the SCB (Li and Li, 2007; Li et al., 2007). However, there are newly discovered Late Triassic (224–215 Ma) A-type granites that are distributed along Zhenghe-Dapu Fault in coastal region of the SCB (Sun et al., 2011, and references therein). The oblique subduction and subsequent roll-back of Paleo-Pacific model was mainly based on the age of Late Mesozoic granitic rocks becomes younger from the inland (Jurassic) toward the coastal area (Cretaceous) (Zhou and Li, 2000; Jiang et al., 2009, 2015). However, recent studies revealed that Jurassic granites also have been identified in the coastal area of the SCB (Zhang et al., 2015b, and references therein). In short, tectonic regime about the direction and subduction angle of Paleo-Pacific plate is enigmatic and controversial. Regardless of the mechanism, underplating of mantle-derived magmas caused by subduction of Paleo-Pacific plate would have provided most of the heat and some of the material required for the widespread Late Mesozoic granitic magmatism in the SCB (Fig. 11c and d).

Mesozoic I- and A-type granites in Guangdong province overall have lower zircon $\delta^{18}O$ values (4.9‰–9.3‰ and 6.8‰–10.6‰, respectively) and more depleted whole-rock Nd ($\varepsilon_{Nd}(t) = -12.3$ to $+1.5$ and -12.1 to -8.1, respectively) and zircon Hf isotopic ($\varepsilon_{Hf}(t) = -14.2$ to $+13.3$ and -17.2 to -4.2, respectively) compositions compared with Mesozoic S-type granites (Figs. 9 and 10; Supplementary Table 5). These I- and A-type granites were formed by partial melting of juvenile crustal rocks (Huang et al., 2013a; Liu et al., 2015; Zhou et al., 2018) or by mixing of crustal metaigneous-rock-derived felsic magmas with mantle-derived mafic magmas (Li et al., 2007; Zhang et al., 2015b; Zheng et al., 2017; Liu et al., 2018; Qing et al., 2020). However, Late Jurassic (ca. 160 Ma) granites in the Guangzhou area are S-type granites that were derived predominantly from partial melting of middle-lower crustal metasedimentary rocks (Liu et al., 2020b, 2021; this study). In addition, Late Jurassic (ca. 160 Ma) syenite porphyries in the Huolushan forest park of Guangzhou area were formed by magma mixing of metasedimentary-rock-derived felsic magmas with minor mantle-derived mafic alkaline magmas (Liu et al., 2020b). Therefore, our study shows that reworking of metasedimentary rocks of the Guangzhou area of SE WYO could have been induced by heating from mantle-derived mafic magmas.

5. Conclusions

(1) LA–ICP–MS zircon U–Pb ages indicate that biotite granodiorites and biotite granites in the Guangzhou area of SE WYO were formed during the Early Silurian (442 Ma) and the Late Jurassic (164–159 Ma), respectively.
(2) Early Silurian biotite granodiorites were formed by partial melting of amphibolites, whereas Late Jurassic biotite granites were formed by partial melting of a hybridized crustal source containing metasedimentary rocks with subordinate juvenile crustal rocks.
(3) The Guangzhou area of SE WYO underwent predominantly middle- to lower-crustal reworking in response to double-thickening of crust during the Late Ordovician to Early Silurian. In addition, during the Late Jurassic, the area underwent reworking mainly of middle- to lower-crustal metasedimentary rocks, which was induced by heating from mantle-derived mafic magmas.

Declaration of Competing Interest

The authors declare that they have no known competing financial interests or personal relationships that could have appeared to influence the work reported in this paper.

Acknowledgements

We thank Editor-in-Chief Mei-Fu Zhou and two anonymous reviewers, whose constructive criticisms and suggestions enabled us to significantly improve this paper. We appreciate the assistance of Lin-Li Chen, Xin-Yu Wang, and Wan-Long Hu during the whole-rock and mineral major element analyses and zircon CL imaging. Xiang-Lin Tu, Sheng-Ling Sun, Wen Zeng, Le Zhang, and Wan-Long Hu are thanked for their help with the whole-rock trace element and Sr–Nd isotope and zircon Hf isotope analyses. We also thank Ya-Nan Yang, Qing Yang, Miao-Hong He, Wan-Long Hu, Zi-Long Wang, Tong-Yu Huang, Qi-Fan Geng, and Yue-Heng Yang for their assistance with LA–ICP–MS zircon U–Pb dating and SIMS zircon O isotope analyses. Wei Dan is thanked for his helpful suggestions and discussions. Financial support for this research was provided by the National Natural Science Foundation of China (42021002), the Key Program of Guangzhou City (No. 201707020032),the Youth Innovation Promotion Association CAS (2017404), and the Pearl River S&T Nova Program of Guangzhou (201906010053). This is contribution IS–3050 from GIGCAS.

Appendix A. Supplementary data

Supplementary data to this article can be found online at https://doi.org/10.1016/j.jseaes.2021.104890.

References

Beard, J., Lofgren, G., 1991. Dehydration melting and water-saturated melting of basaltic and andesitic greenstones and amphibolites at 1, 3, and 6.9 kb. J. Petrol. 32, 365–401.

Cai, D.W., Tang, Y., Zhang, H., Lv, Z.H., Liu, Y.L., 2017. Petrogenesis and tectonic setting of the Devonian Xiqin A-type granite in the northeastern Cathaysia Block, SE China. J. Asian Earth Sci. 141, 43–58.

Cao, J.J., Hu, R.Z., Xie, G.Q., Liu, S., 2009. Geochemistry and genesis of mafic dikes from the coastal areas of Guangdong Province, China. Acta Petrologica Sinica 25, 984–1000 (in Chinese with English abstract).

Chappell, B.W., Bryant, C.J., Wyborn, D., 2012. Peraluminous I-type granites. Lithos 153, 142–153.

Chen, J.F., Jahn, B.M., 1998. Crustal evolution of southeastern China: Nd and Sr isotopic evidence. Tectonophysics 284, 101–133.

Chen, X., Zhang, Y.D., Fan, J.X., Cheng, J.F., Li, Q.J., 2010. Ordovician graptolite-bearing strata in southern Jiangxi with a special reference to the Kwangsian orogeny. Science China Earth Science 53, 1602–1610.

Chappell, B.W., White, A.J.R., 2001. Two contrasting granite types: 25 years later. Austr. J. Earth Sci. 48, 489–499.

Chen, Y.W., Bi, X.W., Hu, R.Z., Dong, S.H., 2012. Element geochemistry, mineralogy, geochronology and zircon Hf isotope of the Luxi and XIazhuang granites in Guangdong province, China: Implications for U mineralization. Lithos 150, 119–134.

Cheng, Hai, 2020. Future earth and sustainable developments. The Innovation 1 (3), 100055. https://doi.org/10.1016/j.xinn.2020.100055.

Ding, X., Zhou, X.M., Sun, T., 2005. The episodic growth of the continental crustal basement in South China: single zircon LA-ICPMS U-Pb dating of Guzhai

granodiorite in Guangdong. Geological Review 51, 382–392 (in Chinese with English abstract).
Faure, M., Shu, L.S., Wang, B., Charvet, J., Choulet, F., Monié, P., 2009. Intracontinental subduction: a possible mechanism for the Early Palaeozoic Orogen of SE China. Terra Nova 21, 360–368.
Feng, S.J., Zhao, K.D., Ling, H.F., Chen, P.R., Chen, W.F., Sun, T., Jiang, S.Y., Pu, W., 2014. Geochronology, elemental and Nd–Hf isotopic geochemistry of Devonian A-type granites in central Jiangxi, South China: Constraints on petrogenesis and post-collisional extension of the Wuyi-Yunkai orogeny. Lithos 206, 1–18.
Gao, P., Zhao, Z.F., Zheng, Y.F., 2014. Petrogenesis of Triassic granites from the Nanling Range in South China: implications for geochemical diversity in granites. Lithos 210–211, 40–56.
Gao, P., Zheng, Y.F., Zhao, Z.F., 2017. Triassic granites in South China: A geochemical perspective on their characteristics, petrogenesis, and tectonic significance. Earth Sci. Rev. 173, 266–294.
GDGBMR (Bureau of Geology and Mineral Resources of Guangdong Province), 1988. Regional Geology of Guangdong Province. Geological Publishing House, Beijing, p. 941.
Guo, X.F., Tian, Y., Zhang, X.B., 2019. Geochronology, genesis and landscape of Yanshanian granite in Guangzhou area, central Guangdong Province of China. SN Applied Sciences 1, 1–11.
Guo, Z.F., Wilson, M., 2012. The Himalayan leucogranites: constraints on the nature of their crustal source region and geodynamic setting. Gondwana Res. 22, 360–376.
Hawkesworth, C.J., Kemp, A.I.S., 2006. Evolution of the continental crust. Nature 443, 811–817.
Holdsworth, R.E., Handa, M., Miller, J.A., Buick, I.S., 2001. Continental reactivation and reworking: an introduction. Geological Society, London, Special Publications 184, 1–12.
Hopkinson, T.N., Harris, N.B., Warren, C.J., Spencer, C.J., Roberts, N.M., Horstwood, M. S., Parrish, R.R., 2017. The identification and significance of pure sediment-derived granites. Earth Planet. Sci. Lett. 467, 57–63.
Hoskin, P., Black, L., 2000. Metamorphic zircon formation by solid-state recrystallization of protolith igneous zircon. J. Metamorph. Geol. 18, 423–439.
Huang, H.Q., Li, X.H., Li, W.X., Li, Z.X., 2011. Formation of high δ^{18}O fayalite-bearing A-type granite by high-temperature melting of granulitic metasedimentary rocks, southern China. Geology 39, 903–906.
Huang, H.Q., Li, X.H., Li, Z.X., Li, W.X., 2013a. Intraplate crustal remelting as the genesis of Jurassic high-K granites in the coastal region of the Guangdong Province, SE China. J. Asian Earth Sci. 74, 280–302.
Huang, H.Q., Li, X.H., Li, Z.X., Li, W.X., 2015. Formation of the Jurassic South China Large Granitic Province: insights from the genesis of the Jiufeng pluton. Chem. Geol. 401, 43–58.
Huang, X.L., Yu, Y., Li, J., Tong, L.X., Chen, L.L., 2013b. Geochronology and petrogenesis of the early Paleozoic I-type granite in the Taishan area, South China: middle-lower crustal melting during orogenic collapse. Lithos 177, 268–284.
Jia, L.H., Mao, J.W., Liu, P., Li, Y., 2018. Petrogenesis of the late Early Cretaceous granodiorite-Quartz diorite from eastern Guangdong, SE China: Implications for tectono-magmatic evolution and porphyry Cu-Au-Mo mineralization. Lithos 304–307, 388–411.
Jia, L.H., Mao, J.W., Liu, P., Yu, M., 2020. Crust-mantle interaction during subduction zone processes: Insight from late Mesozoic I-type granites in eastern Guangdong, SE China. J. Asian Earth Sci. 192, 104284.
Jiang, H., Jiang, S.Y., Li, W.Q., Zhao, K.D., Peng, N.J., 2018. Highly fractionated Jurassic I-type granites and related tungsten mineralization in the Shirenzhang deposit, northern Guangdong, South China: Evidence from cassiterite and zircon U-Pb ages, geochemistry and Sr-Nd-Pb-Hf isotopes. Lithos 312–313, 186–203.
Jiang, H., Jiang, S.Y., Zhao, K.D., Li, W.Q., 2020. Origin of paleosubduction-modified mantle for Late Cretaceous (~100 Ma) diabase in northern Guangdong, South China: Geochronological and geochemical evidence. Lithos 370–371, 105603.
Jiang, Y.H., Jiang, S.Y., Dai, B.Z., Liao, S.Y., Zhao, K.D., Ling, H.F., 2009. Middle to late Jurassic felsic and mafic magmatism in southern Hunan province, southeast China: Implications for a continental arc to rifting. Lithos 107, 185–204.
Jiang, Y.H., Wang, G.C., Liu, Z., Ni, C.Y., Qing, L., Zhang, Q., 2015. Repeated slab advance–retreat of the Palaeo-Pacific plate underneath SE China. Int. Geol. Rev. 57, 472–491.
Jiang, Y.H., Zhu, S.Q., 2017. Petrogenesis of the Late Jurassic peraluminous biotite granites and muscovite-bearing granites in SE China: geochronological, elemental and Sr–Nd–O–Hf isotopic constraints. Contrib. Miner. Petrol. 172, 1–27.
Jiao, S.J., Li, X.H., Huang, H.Q., Deng, X.G., 2015. Metasedimentary melting in the formation of charnockite: Petrological and zircon U-Pb-Hf-O isotope evidence from the Darongshan S-type granitic complex in southern China. Lithos 239, 217–233.
Kemp, A.I.S., Hawkesworth, C.J., Paterson, B.A., Foster, G.L., Kinny, P.D., Whitehouse, M.J., Maas, R., 2008. Exploring the plutonic-volcanic link: a zircon U-Pb, Lu-Hf and O isotope study of paired volcanic and granitic units from southeastern Australia. Earth and Environmental Science Transactions of the Royal Society of Edinburgh 97, 337–355.
Li, W.X., Li, X.H., Li, Z.X., 2005. Neoproterozoic bimodal magmatism in the Cathaysia Block of South China and its tectonic significance. Precambr. Res. 136, 51–66.
Li, X.H., Chen, Z.G., Liu, D.Y., Li, W.X., 2003. Jurassic gabbro-granite-syenite suites from Southern Jiangxi Province, SE China: age, origin, and tectonic significance. Int. Geol. Rev. 45, 898–921.
Li, X.H., Li, W.X., Li, Z.X., Lo, C.H., Wang, J., Ye, M.F., Yang, Y.H., 2009a. Amalgamation between the Yangtze and Cathaysia Blocks in South China: constraints from SHRIMP U-Pb zircon ages, geochemistry and Nd–Hf isotopes of the Shuangxiwu volcanic rocks. Precambr. Res. 174, 117–128.
Li, X.H., Li, W.X., Wang, X.C., Li, Q.L., Liu, Y., Tang, G.Q., 2009b. Role of mantle-derived magma in genesis of early Yanshanian granites in the Nanling Range, South China: in situ zircon Hf-O isotopic constraints. Sci. China, Ser. D Earth Sci. 52, 1262–1278.
Li, X.H., Li, Z.X., Li, W.X., Liu, Y., Yuan, C., Wei, G.J., Qi, C.S., 2007. U-Pb zircon, geochemical and Sr–Nd–Hf isotopic constraints on age and origin of Jurassic I- and A-type granites from central Guangdong, SE China: a major igneous event in response to foundering of a subducted flat-slab? Lithos 96, 186–204.
Li, Z.X., Li, X.H., 2007. Formation of the 1300-km-wide intracontinental orogen and postorogenic magmatic province in Mesozoic South China: a flat-slab subduction model. Geology 35, 179–182.
Li, Z.X., Li, X.H., Wartho, J.A., Clark, C., Li, W.X., Zhang, C.L., Bao, C.M., 2010. Magmatic and metamorphic events during the early Paleozoic Wuyi-Yunkai orogeny, southeastern South China: New age constraints and pressure-temperature conditions. Geol. Soc. Am. Bull. 122, 772–793.
Lin, S.F., Xing, G.F., Davis, D.W., Yin, C.Q., Wu, M.L., Li, L.M., Jiang, Y., Chen, Z.H., 2018. Appalachian-style multi-terrane Wilson cycle model for the assembly of South China. Geology 46, 319–322.
Liu, L., Xu, X.S., Zou, H.B., 2012. Episodic eruptions of the Late Mesozoic volcanic sequences in southeastern Zhejiang, SE China: Petrogenesis and implications for the geodynamics of paleo-Pacific subduction. Lithos 154, 166–180.
Liu, P., Chen, Y.B., Mao, J.W., Wang, X.Y., Yao, W., Cheng, X.T., Zeng, X.J., 2015. Zircon U-Pb age and Hf isotopic characteristics of granite from the Tiandong Tungsten-Sn polymetallic deposit in eastern Guangdong province and its significance. Acta Geol. Sin. 89, 1244–1257 (in Chinese with English abstract).
Liu, P., Mao, J.W., Cheng, Y.B., Yao, W., Wang, X.Y., Hao, D., 2017a. An Early Cretaceous W-Sn deposit and its implications in southeast coastal metallogenic belt: Constraints from U-Pb, Re-Os, Ar-Ar geochronology at the Feie'shan W-Sn deposit, SE China. Ore Geology Review 81, 112–122.
Liu, P., Mao, J.W., Pirajno, F., Jia, L.H., Zhang, F., Li, Y., 2017b. Ore genesis and geodynamic setting of the Lianhuashan porphyry tungsten, eastern Guangdong Province, SE China: constraints from muscovite ^{40}Ar-^{39}Ar and zircon U-Pb dating and Hf isotopes. Ore Geology Review 81, 112–122.
Liu, P., Mao, J.W., Santosh, M., Bao, Z.A., Zeng, X.J., Jia, L.H., 2018. Geochronology and petrogenesis of the Early Cretaceous A-type granite from the Feie'shan W-Sn deposit in the eastern Guangdong Province, SE China: Implications for W-Sn mineralization and geodynamic setting. Lithos 300–301, 330–347.
Liu, Xiao, Wang, Qiang, Ma, Lin, Wyman, Derek, Zhao, Zhen-Hua, Yang, Jin-Hui, Zi, Feng, Tang, Gong-Jian, Dan, Wei, Zhou, Jin-Sheng, 2020c. Petrogenesis of Late Jurassic Pb–Zn mineralized high δ^{18}O granodiorites in the western Nanling Range, South China. J. Asian Earth Sci. 192, 104236.
Liu, X., Wang, Q., Ma, L., Yang, J.H., Gou, G.N., Ou, Q., Wang, J., 2020a. Early Paleozoic intracontinental granites in the Guangzhou region of South China: partial melting of a metasediment-dominated crustal source. Lithos 376–377, 105763.
Liu, X., Wang, Q., Ma, L., Yang, Z.Y., Hu, W.L., Ma, Y.M., Wang, J., Huang, T.Y., 2020b. Petrogenesis of Late Jurassic two-mica granites and associated diorites and syenite porphyries in Guangzhou. SE China. Lithos. 364–365, 105537.
Liu, X., Wang, Q., Ma, L., Gou, G.N., Ou, Q., Wang, J., 2021. Late Jurassic Maofengshan two-mica granites in Guangzhou, South China: Products of the partial melting of metasedimentary rocks. Mineral. Petrol. 115, 1–19.
Ma, L., Wang, Q., Kerr, A.C., Yang, J.H., Xia, X.P., Ou, Q., Yang, Z.Y., Sun, P., 2017. Paleocene (ca. 62 Ma) Leucogranites in Southern Lhasa, Tibet: Products of Syn-collisional Crustal Anatexis during Slab Roll-back? J. Petrol. 58, 2089–2114.
Mao, J.R., Ye, H.M., Liu, K., Li, Z.L., Takahashi, Y., Zhao, X.L., Kee, W.S., 2013a. The Indosinian collision-extension event between the South China Block and the Paleozoic-Pacific plate: Evidence from Indosinian alkaline granitic rocks in Dashuang, eastern Zhejiang, South China. Lithos 172–173, 81–97.
Mao, J.W., Cheng, Y.B., Chen, M.H., Pirajno, F., 2013b. Major types and time–space distribution of Mesozoic ore deposits in South China and their geodynamic settings. Miner. Deposita 48, 267–294.
Mao, J.W., Zheng, W., Xie, G.Q., Lehmann, B., Goldfarb, R., 2021. Recognition of a Middle-Late Jurassic arc-related porphyry copper belt along the southeast China coast: Geological characteristics and metallogenic implications. Geology 49, 1–5.
Mason, Emily, Marie, Edmonds, Alexandra V., Turchyn, 2017. Remobilization of crustal carbon may dominate volcanic arc emissions. Science 357 (6348), 290–294.
Patiño Douce, A.E., 1999. What do experiments tell us about the relative contributions of crust and mantle to the origin of granitic magmas? Geological Society, London, Special Publications 168, 55–75.
Patiño Douce, A.E., Harris, N., 1998. Experimental constraints on Himalayan anatexis. J. Petrol. 39, 689–710.
Patiño Douce, A.E., Johnston, A.D., 1991. Phase equilibria and melt productivity in the pelitic system: implications for the origin of peraluminous granitoids and aluminous granulites. Contrib. Miner. Petrol. 107, 202–218.
Patiño Douce, A.E., Beard, J.S., 1995. Dehydration-melting of biotite gneiss and quartz amphibolite from 3 to 15 kbar. J. Petrol. 36, 707–738.
Peng, B.X., Wang, Y.J., Fan, W.M., Peng, T.P., Liang, X.Q., 2006. LA-ICPMS zircon U-Pb dating for three Indosinian granitic plutons from central Hunan and western Guangdong provinces and its petrogenetic implications. Acta Geol. Sin. 80, 660–669.
Qing, L., Jiang, Y.H., Du, F.G., 2020. Petrogenesis and tectonic significance of early Indosinian A-type granites in the Xinxing pluton, southern South China. Mineral. Petrol. 114, 217–242.
Qiu, Z.W., Li, S.S., Yan, Q.H., Wang, H., Wei, X.P., Li, P., Wang, L.M., Bu, A., 2017a. Late Jurassic Sn metallogeny in eastern Guangdong, SE China coast: Evidence from geochronology, geochemistry and Sr-Nd-Hf-S isotopes of the Dadaoshan Sn deposit. Ore Geology Review 83, 63–83.
Qiu, Z.W., Yan, Q.H., Li, S.S., Wang, H., Tong, L.X., Zhang, R.Q., Wei, X.P., Li, P., Wang, L.M., Bu, A., Yan, L.M., 2017b. Highly fractionated Early Cretaceous I-type

granites and related Sn polymetallic mineralization in the Jinkeng deposit, eastern Guangdong, SE China: Constraints from geochronology, geochemistry, and Hf isotopes. Ore Geology Review 88, 718–738.
Rong, W., Zhang, S.B., Zheng, Y.F., 2017. Back-reaction of peritectic garnet as an explanation for the origin of mafic enclaves in S-type granite from the Jiuling batholith in South China. J. Petrol. 58, 569–598.
Sawyer, E.W., Cesare, B., Brown, M., 2011. When the continental crust melts. Elements 7, 229–233.
Shen, W.Z., Ling, H.F., Li, W.X., Wang, D.Z., Huang, X., Pan, J., 1999. Nd-Sr isotopic study of Mesozoic granitoids in Jiangxi Province. Chin. Sci. Bull. 44, 1427–1431.
Shu, L.S., Song, M.J., Yao, J.L., 2018. Appalachian-style multi-terrane Wilson cycle model for the assembly of South China: COMMENT. Geology 46, e445.
Shu, L.S., Wang, B., Cawood, P.A., Santosh, M., Xu, Z.Q., 2015. Early Paleozoic and Early Mesozoic intraplate tectonic and magmatic events in the Cathaysia Block, South China. Tectonics 34, 1600–1621.
Shu, L.S., Wang, J.Q., Yao, J.L., 2019. Tectonic evolution of the eastern Jiangnan region, South China: new findings and implications on the assembly of the Rodinia supercontinent. Precambr. Res. 322, 42–65.
Shu, L.S., Yao, J.Q., Wang, B., Faure, M., Charvet, J., Chen, Y., 2021. Neoproterozoic plate tectonic process and Phanerozoic geodynamic evolution of the South China Block. Earth-Science Review 216, 103596.
Shu, X.J., Wang, X.L., Sun, T., Xu, X.S., Dai, M.N., 2011. Trace element, U-Pb ages and Hf isotopes of zircons from Mesozoic granites in the western Nanling Range, South China: Implications for petrogenesis and W-Sn mineralization. Lithos 127, 468–482.
Sisson, T.W., Ratajeski, K., Hankins, W.B., Glazner, A.F., 2005. Voluminous granitic magmas from common basaltic sources. Contrib. Miner. Petrol. 148, 635–661.
Sun, S.-S., McDonough, W.F., 1989. Chemical and isotopic systematics of oceanic basalts: implications for mantle composition and processes. Geological Society, London, Special Publications 42, 313–345.
Sun, Y., Ma, C.Q., Liu, Y.Y., She, Z.B., 2011. Geochronological and geochemical constraints on the petrogenesis of late Triassic aluminous A-type granites in southeast China. J. Asian Earth Sci. 42, 1117–1131.
Tang, G.J., Wang, Q., Zhang, C.F., Wyman, Derek A., Dan, W., Xia, X.P., Chen, H.Y., Zhao, Z.H., 2017. Sr-Nd-Hf-O isotope geochemistry of the Ertaibei pluton, East Junggar, NW China: Implications for development of a crustal-scale granitoid pluton and crustal growth. Geochem. Geophys. Geosyst. 18, 3340–3358.
Tong, L.X., Li, C., Liu, Z., Zhai, M.G., Li, W.X., 2021. First report of phengites in the Longyou paragneiss in the northern Early Paleozoic Wuyi-Yunkai orogen, South China: P-T conditions, zircon U-Pb ages and tectonic implications. J. Asian Earth Sci. 214, 104754.
Wang, D., Zheng, J.P., Ma, Q., Griffin, W.L., Zhao, H., Wong, J., 2013a. Early Paleozoic crustal anatexis in the intraplate Wuyi-Yunkai orogen, South China. Lithos 175–176, 124–145.
Wang, J., Li, Z.X., 2003. History of Neoproterozoic rift basins in South China: implications for Rodinia breakup. Precambr. Res. 122, 141–158.
Wang, Y.J., Fan, W.M., Guo, F., Peng, T.P., Li, C.W., 2003. Geochemistry of Mesozoic mafic rocks adjacent to the Chenzhou-Linwu fault, South China: implications for the lithospheric boundary between the Yangtze and Cathaysia blocks. Int. Geol. Rev. 45, 263–286.
Wang, Y.J., Fan, W.M., Sun, M., Liang, X.Q., Zhang, Y.H., Peng, T.P., 2007a. Geochronological, geochemical and geothermal constraints on petrogenesis of the Indosinian peraluminous granites in the South China Block: a case study in the Hunan Province. Lithos 96, 475–502.
Wang, Y.J., Fan, W.M., Zhao, G.C., Ji, S.C., Peng, T.P., 2007b. Zircon U-Pb geochronology of gneissic rocks in the Yunkai massif and its implications on the Caledonian event in the South China Block. Gondwana Res. 12, 404–416.
Wang, Y.J., Fan, W.M., Zhang, G.W., Zhang, Y.H., 2013b. Phanerozoic tectonics of the South China Block: key observations and controversies. Gondwana Res. 23, 1273–1305.
Wang, Y.J., Zhang, A.M., Fan, W.M., Zhang, Y.H., Zhang, Y.Z., 2013c. Origin of paleosubduction-modified mantle for Silurian gabbro in the Cathaysia Block: geochronological and geochemical evidence. Lithos 160, 37–54.
Wang, Y.J., Zhang, A.M., Fan, W.M., Zhao, G.C., Zhang, G.W., Zhang, Y.Z., Zhang, F.F., Li, S.Z., 2011. Kwangsian crustal anatexis within the eastern South China Block: geochemical, zircon U-Pb geochronological and Hf isotopic fingerprints from the gneissoid granites of Wugong and Wuyi-Yunkai Domains. Lithos 127, 239–260.
Whitney, D.L., Evans, B.W., 2010. Abbreviations for names of rock-forming minerals. Am. Mineral. 95, 185–187.
Xia, Y., Xu, X.S., Zou, H.B., Liu, L., 2014. Early Paleozoic crust–mantle interaction and lithosphere delamination in South China Block: evidence from geochronology, geochemistry, and Sr–Nd–Hf isotopes of granites. Lithos 184, 416–435.
Xie, Y.X., Ma, L.Y., Zhao, G.C., Xie, C.F., Han, Y.G., Li, J.H., Liu, Q., Yao, J.L., Zhang, Y. Y., Lu, Y.F., 2020. Origin of the Heping granodiorite pluton: Implications for syn-convergent extension and asthenosphere upwelling accompanying the early Paleozoic orogeny in South China. Gondwana Res. 85, 149–168.
Xin, Y.J., Li, J.H., Ratschbacher, L., Zhao, G.C., Zhang, Y.Q., Dong, S.W., Xia, X.P., Yu, Y. Q., 2020. Early Devonian (415–400 Ma) A-type granitoids and diabases in the Wuyishan, eastern Cathaysia: A signal of crustal extension coeval with the separation of South China from Gondwana. Geological Society of American Bulletin 132, 2295–2317.
Xu, X.S., Reilly, S.Y.O., Griffin, W.L., Deng, P., Pearson, N.J., 2005. Relict Proterozoic basement in the Nanling Mountains (SE China) and its tectonothermal overprinting. Tectonics 24, 1–16.
Yan, Q.H., Li, S.S., Qiu, Z.W., Wang, H., Wei, X.P., Li, P., Dong, R., Zhang, X.Y., 2017. Geochronology, geochemistry and Sr-Nd-Hf-S-Pb isotopes of the Early Cretaceous Taoxihu Sn deposit and related granitoids, SE China. Ore Geology Review 89, 350–368.
Yang, D.S., Li, X.H., Li, W.X., Liang, X.Q., Long, W.G., Xiong, X.L., 2010. U-Pb and ^{40}Ar–^{39}Ar geochronology of the Baiyunshan gneiss (central Guangdong, south China): constraints on the timing of early Palaeozoic and Mesozoic tectonothermal events in the Wuyun (Wuyi-Yunkai) Orogen. Geol. Mag. 147, 481–496.
Yang, Z.Y., Wang, Q., Hao, L.L., Wyman, D.A., Ma, L., Wang, J., Qi, Y., Sun, P., Hu, W.L., 2021. Subduction erosion and crustal material recycling indicated by adakites in central Tibet. Geology 49, 1–5.
Yao, W.H., Li, Z.X., Li, W.X., Wang, X.C., Li, X.H., Yang, J.H., 2012. Post-kinematic lithospheric delamination of the Wuyi-Yunkai orogen in South China: evidence from ca. 435 Ma high-Mg basalts. Lithos 154, 115–129.
Yu, P.P., Zhang, Y.Z., Zhou, Y.Z., Weinberg, R.F., Zheng, Y., Yang, W.B., 2019. Melt evolution of crustal anatexis recorded by the Early Paleozoic Baiyunshan migmatite-granite suite in South China. Lithos 332–333, 83–98.
Yu, Y., Huang, X.L., Sun, M., He, P.L., 2018. Petrogenesis of granitoids and associated xenoliths in the Early Paleozoic Baoxu and Enping plutons, South China: implications for the evolution of the Wuyi-Yunkai intracontinental orogen. J. Asian Earth Sci. 156, 59–74.
Yuan, Z.X., Wu, L.S., Zhang, Z.Q., Ye, X.J., 1991. The Sm-Nd, Rb-Sr isotopic age-dating of Mayuan group in northern Fujian. Acta Petrologica et Mineralogica 10, 127–132 (in Chinese with English abstract).
Zhang, F.F., Wang, Y.J., Zhang, A.M., Fan, W.M., Zhang, Y.Z., Zi, J.W., 2012. Geochronological and geochemical constraints on the petrogenesis of Middle Paleozoic (Kwangsian) massive granites in the eastern South China Block. Lithos 150, 188–208.
Zhang, Q., Jiang, Y.H., Wang, G.C., Liu, Z., Ni, C.Y., Qing, L., 2015a. Origin of Silurian gabbros and I-type granites in central Fujian, SE China: implications for the evolution of the early Paleozoic orogen of South China. Lithos 216, 285–297.
Zhang, Y., Yang, J.H., Sun, J.F., Zhang, J.H., Chen, J.Y., Li, X.H., 2015b. Petrogenesis of Jurassic fractionated I-type granites in Southeast China: Constraints from whole-rock geochemical and zircon U-Pb and Hf–O isotopes. J. Asian Earth Sci. 111, 268–283.
Zhao, G.C., 2015. Jiangnan Orogen in South China: developing from divergent double subduction. Gondwana Res. 27, 1173–1180.
Zhao, Z.F., Zheng, Y.F., Wei, C.S., Wu, Y.B., 2007. Post-collisional granitoids from the Dabie orogen in China: Zircon U-Pb age, element and O isotope evidence for recycling of subducted continental crust. Lithos 93, 248–272.
Zheng, W., Mao, J.W., Zhao, H.J., Zhao, C.S., Yu, X.F., 2017. Two Late Cretaceous A-type granites related to the Yingwuling W-Sn polymetallic mineralization in Guangdong province, South China: Implications for petrogenesis, geodynamic setting, and mineralization. Lithos 274–275, 106–122.
Zheng, Y.F., Zhang, S.B., Zhao, Z.F., Wu, Y.B., Li, X.H., Li, Z.X., Wu, F.Y., 2007. Contrasting zircon Hf and O isotopes in the two episodes of Neoproterozoic granitoids in South China: implications for growth and reworking of continental crust. Lithos 96, 127–150.
Zhong, Y.F., Ma, C.Q., Liu, L., Zhao, J.H., Zheng, J.P., Nong, J.N., Zhang, Z.J., 2014. Ordovician appinites in the Wugongshan Domain of the Cathaysia Block, South China: Geochronological and geochemical evidence for intrusion into a local extensional zone within an intracontinental regime. Lithos 198, 202–216.
Zhong, Y.F., Wang, L.X., Zhao, J.H., Liu, L., Ma, C.Q., Zheng, J.P., Zheng, Z.J., Luo, B.J., 2016. Partial melting of an ancient sub-continental lithospheric mantle in the early Paleozoic intracontinental regime and its contribution to petrogenesis of the coeval peraluminous granites in South China. Lithos 264, 224–238.
Zhou, X.M., Li, W.X., 2000. Origin of Late Mesozoic igneous rocks in Southeastern China: implications for lithosphere subduction and underplating of mafic magmas. Tectonophysics 326, 269–287.
Zhou, X.M., Sun, T., Shen, W.Z., Shu, L.S., Niu, Y.L., 2006. Petrogenesis of Mesozoic granitoids and volcanic rocks in South China: a response to tectonic evolution. Episodes 29, 26–33.
Zhou, Z.M., Ma, C.Q., Wang, L.X., Chen, S.G., Xie, C.F., Li, Y., Liu, W., 2018. A source-depleted Early Jurassic granitic pluton from South China: Implication to the Mesozoic juvenile accretion of the South China crust. Lithos 300–301, 278–290.
Zhu, W.G., Zhong, H., Li, X.H., He, D.F., Song, X.Y., Ren, T., Chen, Z.Q., Sun, H.S., Liao, J. Q., 2010. The early Jurassic mafic-ultramafic intrusion and A-type granite from northeastern Guangdong, SE China: Age, origin, and tectonic significance. Lithos 119, 313–329.